UNIVERSITY OF TURKU

Fabrication methods and electrochemical study of various metallic nanoparticles (NPs)

Materials Engineering in Health Technology
Department of Mechanical and Materials Engineering
Faculty of Technology
Master's thesis

Author(s):
Edna Arlyne De Jesus Cabrera

26.06.2024
Turku

Master's thesis

Subject: Materials Engineering
Author(s): Edna Arlyne De Jesus Cabrera
Title: Fabrication methods and electrochemical study of various metallic nanoparticles (NPs)
Supervisor(s): Professor Emilia Peltola & MSc. Bahar Mostafiz
Number of pages: 58 pages
Date: 26.06.2024

Metallic nanoparticles have size dependent properties that differ from those in bulk materials. Controlling the synthesis process is crucial to achieve various sizes and shapes. Depending on the size, metallic nanoparticles have properties that can be incorporated across several industries like pharmaceuticals, diagnostics, sensing, etc. Moreover, the electrochemical behaviour of an electrode may differ when different types of metallic nanoparticles are placed on its active surface.

This thesis aims to synthesize various types of metallic nanoparticles, controlling their size, shape, and composition. Such as nanoparticles made of gold and expanding to gold core nanorods with metals like silver and platinum as shells. Then, the electrochemical behaviour of a glassy carbon electrode (GCE) would be studied by modifying the electrode with the final synthesis products.

Synthesis of different shaped gold nanoparticles took place with non-seeding and seed-mediated growth methods. Capsule-shaped core@shell gold, silver, and platinum nanorods were synthesized with a non-seeding, colloid stabilizing and galvanic replacement method. The synthesized nanomaterials were characterized with UV-Vis spectroscopy and transmission electron microscopy (TEM). Followed by drop casting these various nanomaterials over a glassy carbon electrode (GCE) so that the electrochemical behaviour of the modified electrodes could be studied through cyclic voltammetry (CV) versus both PBS and Ru salt solutions.

The characterization methods revealed different shapes, sizes, and compositions of metallic nanoparticles. Demonstrating how controlling the synthesis process can tailor the fabricated nanomaterials as desired. The electrochemical results showed that the glassy carbon electrode (GCE) behaviour changed when each of the synthesized nanoparticles were placed over its active surface.

The findings in this thesis demonstrated the importance of controlling the synthesis of metallic nanoparticles and the impact they can have on the electrochemical behaviour of a glassy carbon electrode (GCE) when drop casted on their surface. This project has the potential to be expanded by investigating the impact of synthesized nanomaterials on the electrochemical behaviour of the electrode. Additionally, testing the modified electrode with various analytes containing biomolecules for exploring their potential applications in biosensing is a possibility.

Key words: Nanoparticle, Core@shell, Electrode modification, Au@Pt nanoparticles, Nanorods.

Table of Contents

Abbreviations **5**

1 Introduction **6**

2 Nanoparticles **7**

2.1 Metallic nanoparticles **7**

2.1.1 Core@shell metallic nanoparticles 8

2.1.2 Fabrication routes 9

2.2 Upsides & downsides **11**

2.3 Applications **13**

2.3.1 Drug delivery 13

2.3.2 Theranostics 14

2.3.3 Biomedical imaging 14

2.3.4 Biomolecules monitoring 15

3 Electrochemical insights **18**

3.1 Basics of electrochemistry **18**

3.2 Cyclic voltammetry **20**

4 Experimental **22**

4.1 Chemicals & Apparatus **22**

4.2 Synthesis methods **23**

4.2.1 Different aspect ratio gold nanoparticles 23

4.2.2 Bone-shaped gold nanorods 26

4.2.3 Capsule-shaped gold core with platinum shell nanorods 28

4.3 Electrochemical studies **33**

4.3.1 Potential windows 34

4.3.2 Outer sphere redox probe studies 35

5 Results & Discussion **36**

5.1 Nanoparticles characterization **36**

5.1.1 UV-visible spectroscopy 37

5.1.2 Transmission electron microscopy 42

5.2 Electrochemical characterization **46**

5.2.1 Potential windows 47

5.2.2 Outer sphere redox probe studies 50

6 Conclusion 53

References 54

Abbreviations

Term	Meaning
Ag@Pt NPs	Silver core with platinum shell nanoparticles
Au NPs	Gold nanoparticles
Au NPs 2.1 AR	Gold nanoparticles with 2.1 aspect ratio
Au NPs 3.3 AR	Gold nanoparticles with 3.3 aspect ratio
Au NRs	Gold nanorods
Au@Ag NRs	Gold core with silver shell nanorods
Au@Pt NRs	Gold core with platinum shell nanorods
Au@Pt-C NRs	Gold core with continuous platinum shell nanorods
Au@Pt-DC NRs	Gold core with discontinuous platinum shell nanorods
CE	Counter electrode
CT	Computed tomography
CV	Cyclic voltammetry
DPV	Differential pulse voltammetry
EIS	Electrochemical impedance spectroscopy
FT-IR	Fourier transform infrared
GCE	Glassy carbon electrode
GO	Graphene oxide
GOx	Glucose oxidase
Gr	Graphene
MRI	Magnetic resonance imaging
NPs	Nanoparticles
NRs	Nanorods
PANI	Polyaniline
PBS	Phosphate buffered saline
PW	Potential window
RE	Reference electrode
SCE	Saturated calomel electrode
SEM	Scanning electron microscopy
SPCE	Screen printed carbon electrode
TEM	Transmission electron microscopy
Tf	Transferrin
UV-vis	UV-visible spectroscopy
WE	Working electrode
XPS	X-ray photoelectron spectroscopy

1 Introduction

Nanoscience studies materials and structures in the nanoscale, where unique physicochemical properties emerge due to their size dependency. These materials, better known as nanomaterials, behave differently from those at larger scales due to their surface and quantum effects. As a material decreases in size, there are more atoms in the surface of the now nanomaterial, resulting in a larger surface area where reactions can take place (Joudeh and Linke, 2022; Khan et al., 2019). Thus, enhancing the physicochemical properties of a material, making them exhibit new properties or enhancing those known before. Resulting in an increase of interest in nanomaterials, nanoparticles (NPs) in specific, for their multiple applications across different industries.

Tailoring the size, shape, and composition of metallic NPs is possible by controlling the synthesis process conditions, which can enhance catalytic, conductivity, and optoelectronic properties among others (Saha et al., 2012).

Regarding biomedical applications, noble metallic NPs have gained attention due to their biomolecule like size that holds a promising future in applications like drug delivery, theranostics, biomedical imaging, and biosensors (Yih and Talpasanu, 2008). The most studied metallic NPs in biomedical applications have been Au NPs due to the inertness and biocompatibility of the metal, making it a good option for modifying and developing biomedical devices. For example, sensing devices would benefit from the large surface area for reactions to occur and enhanced conductive properties of Au NPs, since it could result on signal amplification.

This thesis will start with a brief overview on NPs, highlighting metallic NPs and some biomedical applications for them. Moving on to how NPs have been used in electrochemical biosensors modification and the electrochemistry behind their study. The experimental part is composed by the synthesis of various types of metallic NPs, aiming to achieve certain sizes, shapes, and compositions. The metallic NPs will be fabricated with Au, with some NPs coatings consisting of other noble metals. The synthesized shapes will go from spherical NPs to capsule-shaped core@shell NRs. These metallic NPs will be characterized with UV-Vis, transmission electron microscopy (TEM), and cyclic voltammetry (CV). The latter to study how the electrochemical behaviour of a glassy carbon electrode (GCE) changes when modified with nanomaterials in different analytes.

2 Nanoparticles

In this chapter, NPs will be introduced alongside their various types. With metallic NPs being the focus of this study. The advantages and disadvantages of these nanomaterials are discussed, as some of their fabrication methods. The chapter finishes by looking into the applications of NPs across diverse industries.

NPs as a subcategory of nanomaterials, are particles that have at least one dimension in the range between 1 to 100 nm. Several researchers have noted that this type of nanomaterials exhibit properties that differ from those found on bulk materials depending on their size and surface functionalities (Najahi-Missaoui et al., 2020; Wang and Wang, 2014).

When materials reach the nanoscale, new properties can be seen due to constraints on their electronic motion (Huang et al., 2009). The properties are significantly influenced by the size and shape of the nanomaterial due to their anisotropic nature. This has sparked curiosity to investigate how can fabrication methods tune the aspect ratio and shape of NPs to study their various properties and use them in different fields (Huang et al., 2009; Jelinek, 2015; Pérez-Juste et al., 2005).

NPs can be classified in many ways, e.g., by their properties, shape, size, material, fabrication method, etc. There is no standardized classification system, since the focus may differ depending on the research interest and needs. Nevertheless, the most well-known types seen within the NPs ongoing research are carbon-based NPs, metallic NPs, ceramic NPs, semiconductor NPs, polymeric NPs, and lipid-based NPs.

Overall, the use of NPs has been investigated in various areas of research like catalysis, electronics, and biomedical applications like diagnostics, sensing, drug delivery, and therapeutics (Khan et al., 2019; Najahi-Missaoui et al., 2020).

2.1 Metallic nanoparticles

As their name suggests, metallic NPs are composed of metals. They can be monometallic or bimetallic. These nanostructures can be made from alloys or can be monometallic in different layers, also known as core@shell. A significant amount of the metallic NPs research focuses on utilizing gold (Au), silver (Ag), iron (Fe), platinum (Pt), and palladium (Pd) to synthesize the nanostructures.

Metallic NPs possess unique optical and electrical properties, such as absorption and photoluminescence emission, tightly related to their localized surface plasmon resonance

characteristics. Several authors have mentioned that such properties can be tailored by adjusting the aspect ratio, composition or shape of the NP (Jelinek, 2015; Joudeh and Linke, 2022; Khan et al., 2019; Sharma et al., 2016).

However, gold (Au) stands out among the other noble metals due to its biocompatibility, facile synthesis methods with straightforward surface manipulation (Cobley and Xia, 2010), inertness, long-term stability, and heat transport (Chan, 2007; Jelinek, 2015; Joudeh and Linke, 2022), in addition to the previously mentioned properties.

Their nanoscale size enhances these properties due to their high surface to volume ratio, which can be further increased depending on the chosen morphology. As it will be mentioned later, the progress in synthesis methods has allowed to fabricate different shapes from spherical NPs, such as rods, bones, cubes, stars, wires, etc.

2.1.1 Core@shell metallic nanoparticles

Bimetallic NPs, also known as core@shell NPs, are comprised of two different metals. Their structure consists of a core encased within a distinct shell layer. Numerous studies have indicated that core@shell NPs exhibit optical, electronic, magnetic, and catalytic properties that stand out from their bulk metals and their monometallic NPs as well (Guo et al., 2007; Sharma et al., 2016; Srnová-Šloufová et al., 2004; Wang and Wang, 2014). Some of the more commonly synthesized core@shell NPs include Au@Pt, Au@Pd, Au@Ag, Ag@Pt, and Ag@Pd.

Considerable research has been dedicated to control the synthesis methods of core@shell NPs with specific compositions and morphologies since their properties are heavily influenced by their size, shape, and composition.

However, the structure of the NPs complicates by adding an additional layer to it, since the uniformity of the shell becomes of great interest. In this case, a mismatch in the lattice structure, surface, or cohesive energies of the metals in the core@shell NP may cause uneven coatings over the core material. Sharma et al. exemplifies this by describing how a lattice mismatch added to high cohesive and surface energy makes it difficult to achieve a uniform coating of platinum (Pt) over a gold (Au) surface in a Au@Pt NP (Sharma et al., 2016).

Achieving a smooth or uneven shell affects the exhibited properties of the core@shell NPs. The work done by Fennell et al. mentions the popularity gained by Au@Pd and Au@Pt NPs due to their properties that have the potential to produce catalysts with enhanced stability and performance

(Fennell et al., 2013). The catalytic properties of platinum (Pt) have been studied by coating Au NPs with an even and uneven shell of this metal over them, both shell types exhibited enhanced electrochemical activity (Guo et al., 2007; Sharma et al., 2016).

Having the possibility to tune the metallic NPs with core@shell structures, broadens the applications across different fields for this type of nanomaterial. The applications across different industries will be discussed later in this chapter.

2.1.2 Fabrication routes

The synthesis of metallic NPs can be categorized in two approaches: “top-down” or “bottom-up”. The top-down approach includes methods that require tools to make a bulk material achieve a desired shape or size. Some examples of this approach include template methods and lithography methods. Whilst the bottom-up approach benefits from the chemical properties of molecules, letting them self-assemble into a desired shape or size. Some examples of this approach include the seeding method, non-seeding method, and the photochemical method.

Majority of metallic NPs synthesis methods are considered sustainable since in most cases there is no need for high-energy equipment and reactions can take place at room temperature. At the same time, the production of these nanostructures produces less by-products due to the small volumes of chemicals needed to produce large amounts of NPs. However, the focus of this thesis will be on the synthesis methods of Au NPs only.

Each of the previously mentioned methods will be described briefly, including their advantages and disadvantages. However, a summary including this information can be found in Table 1.

Top-down approach

The template method takes place over a polycarbonate or alumina porous template, in which Au will be electrodeposited into the pores of the template using a metal ion precursor analyte. Once the process finishes, the synthesised material is released by dissolving the template. In result, the synthesized material will have the same diameter as the pore diameters, whilst the length of the nanomaterial will vary depending on the amount of gold deposited (Huang et al., 2009; Pérez-Juste et al., 2005; Vigderman et al., 2012). An advantage of this method is the ability to set the diameter and length of the NRs by controlling the pore diameter of the template. The downside of the method is the amount of material that can be synthesized, since it is growth is limited only in monolayers.

The most popular lithography methods to synthesize Au NPs are electron-beam lithography (EBL) and focused ion beam lithography (FIB). These methods use a resist coated substrate or film and with a patterned mask a template is formed over the substrate. Depending on the substrate used, either the unexposed or exposed areas will be removed after being exposed to an electron beam or ion beam. Then the Au precursor is deposited onto the patterned area of the substrate and the NPs are collected by removing the leftover material These synthesis methods can control NPs sizes and shapes with high precision but they are very demanding methods that cannot synthesize structures smaller than 10 nm (Huang et al., 2009).

Bottom-up approach

The electrochemical synthesis method has been widely used to synthesize metallic NPs. In the case of Au NPs, three metal plates, gold (Au), silver (Ag) and platinum (Pt), are immersed in a cosurfactant solution in an electrochemical cell. The redox reaction and presence of the surfactants causes the formation of Au NPs onto the platinum (Pt) plate and once the reaction ends, the Au NPs are taken away from the cathode plate through sonication (Huang et al., 2009; Ma et al., 2004). A huge benefit of this method is the purity of the synthesized NPs and use of less compounds to achieve the nanostructures. Alongside with the control of aspect ratio by controlling the silver plate submersion onto the solution. However, there is still the risk of impurities caused by the surfactants.

The seeding method takes place by having two solutions, a seed and growth solution. The seed solution contains Au precursor solution and a reducing agent. On the other hand, the growth solution contains metal precursor solution, surfactants, and a reducing agent. The aspect ratio of the NPs can be varied depending on the amount of the seed solution added to the growth solution (Lohse and Murphy, 2013; Murphy et al., 2011; Pérez-Juste et al., 2005; Vigderman et al., 2012). This synthesis method is the most popular among the different synthesis methods for Au NPs due to their simple procedure, high number of NPs synthesized, and ability to control the aspect ratio of the nanostructures. However, the purification procedure of surfactants by centrifugation is lengthy, and it is possible to have different shapes or impurities within the synthesized NPs.

Different from the seeding method, the non-seeding method can synthesize Au NPs without the need of a seed solution. The growth solution contains the Au precursor solution, a stabilizer, a surfactant, and a reducing agent. However, in this method a strong reducing agent, like sodium borohydride ($NaBH_4$), is added to the solution so that the metal ions are reduced and aggregated to form Au NPs (Lohse and Murphy, 2013; Vigderman et al., 2012). This method allows controlling the size and shape by varying the concentration and amount of the reactants with a high number of synthesized NPs.

However, there may be different shapes synthesized in the solution, since the method is highly dependent on the quality of sodium borohydride ($NaBH_4$) and may hinder the quality of synthesized NPs.

The photochemical synthesis method uses light to convert an Au precursor solution into NPs with uniform size, this is done by adding the Au precursor solution to a surfactant solution and then irradiating the solution with 254 nm UV-light for around 30 hrs. The NPs are collected through centrifugation and redispersed in water (Kim et al., 2002; Lohse and Murphy, 2013). The aspect ratio of the NPs can be controlled by varying the irradiated UV-light. However, the slow growth rate makes the synthesis processing time lengthy.

Table 1. Fabrication routes of metallic NPs

Method	Advantages	Disadvantages
Template	Diameter and length can be controlled	Growth is limited to monolayers
Lithography	Precise size and shape control	Highly demanding method with size >10 nm limit
Electrodeposition	Pure metallic NPs synthesis, less compounds needed, and aspect ratio control	Risk of impurities
Seeding method	High yield of synthesized NPs, aspect ratio can be controlled, and simple procedure	Lengthy purification process, and risk of non-uniform NPs synthesis
Non-seeding method	Size and shape control, high yield of synthesized NPs	Highly dependent on NaBH4 quality, and risk of non-uniform NPs synthesis
Photochemical method	Uniform NPs size synthesis and simple process	Long process (30 hrs.)

2.2 Upsides & downsides

The nanoscale size and shape have huge impacts on metallic NPs and its effects have been mentioned throughout the entire chapter. The scientific name for this phenomenon is “quantum size effect” where due to the high surface area to volume ratio, the surface atoms on the NPs surface are comparable or even more in number to those found on their bulk materials (Toshima and Yonezawa, 1998).

A high surface to volume ratio leads metallic NPs to have more catalytic, magnetic, electrical and heat conductive properties, since there are more electrons that can undergo transfers in the NP surface

as the size decreases (Cobley and Xia, 2010; Joudeh and Linke, 2022). In the case of catalysis, the size of the nanomaterial will not only boost its activity but will enhance its selectivity as well.

Their optical properties stand out due to their bright colours, which are absent in bulk materials of noble metals like gold and silver; making them exhibit strong, distinctive absorption bands in the visible spectrum (Pérez-Juste et al., 2005).

However, even though there are plenty of academic works mentioning the unique properties and advantages of NPs and their applications; one should not forget to address risks to human health and the environment that could arise from exposure to this type of nanomaterials. These studies mentioned how the size and different behaviour allows NPs to penetrate cell membranes, even cross the blood-brain barrier, and how the body is not able to excrete them entirely so this nanomaterial accumulates in organs instead (Dreaden et al., 2012; Huang et al., 2009; Najahi-Missaoui et al., 2020; Tan et al., 2018). To understand further the risks of NPs, it is important look into the toxicity of the used materials, the biodistribution of this nanomaterial within the human body, and how it is disposed from the body.

Noble metals have been present in several applications throughout history. Yet, when these materials reach the nanoscale, their chemical reactivity differs from the one known in their bulk presentation. Confirming that the size and shape will not only affect the properties of NPs, but their toxicity as well.

These types of metals are overall considered inert and biocompatible, but their synthesis process to becoming NPs with certain properties may include other materials that are considered as toxic. CTAB (hexadecyltrimethyl ammonium bromide) for example, is a popular surfactant used in metallic NPs fabrication processes. A study conducted by Huang et al. showed that whilst free CTAB molecules represent a risk for human cells, bound CTAB molecules are safe; and since unbound molecules of this material can be separated or replaced through different techniques, the synthesized NPs can be used for clinical studies safely (Huang et al., 2009).

The exposure to NPs may occur in different ways, like skin contact, inhalation, ingestion, or injection, at the same time NPs can be found as environmental contaminants so it is possible to be exposed to them unknowingly if they are not properly discarded. Shown in Figure 1, once they enter the human body, they can move around and reach organs like lungs, brain, liver, spleen, and kidneys, depending on the entry route. Some would be able to leave the body, whilst some others could accumulate,

resulting in unwanted reactions like inflammatory responses, fibrosis, or necrosis of tissues exposed to them (Dreaden et al., 2012; Joudeh and Linke, 2022; Najahi-Missaoui et al., 2020).

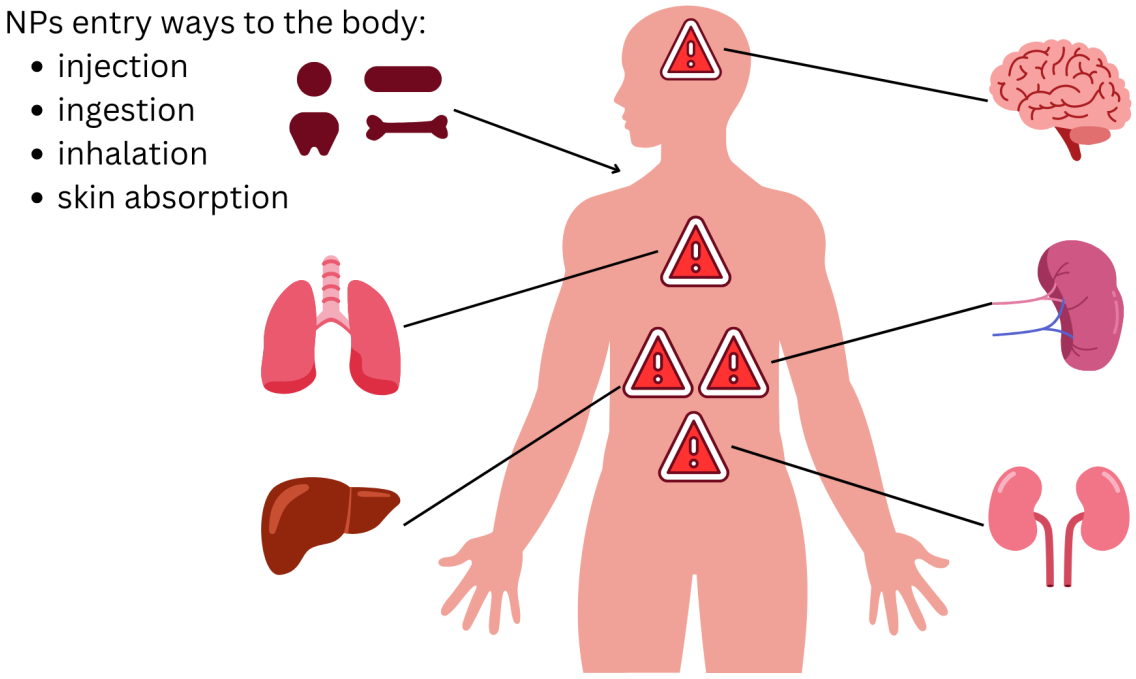

Figure 1. Organs that could be affected by NP accumulation.

The research to understand in full detail the risks that NPs could present to human's wellbeing is still ongoing. Considering the full potential of nanomaterials for biomedical applications cannot be fully studied until it is determined that it is safe for NPs to take part on clinical trials.

2.3 Applications

As mentioned before, NPs have unique physicochemical properties that place them in the spotlight to be incorporated in a wide range of biomedical applications, such as drug delivery, theranostics, biomedical imaging, and biosensing.

2.3.1 Drug delivery

The medical and pharmaceutical sectors are increasingly focusing on NPs due to their capacity to encapsulate materials. This capability allows for the precise delivery of drugs at optimal dosages, tailored for specific treatments or individual patient requirements.

Aiming to achieve a controlled and sustained drug release, research has been focusing on developing biodegradable NPs, with biocompatible materials like polymers or liposomes such as poly lactic

glycolic acid (PLGA) and chitosan (Alexis et al., 2008; Khan et al., 2019; Najahi-Missaoui et al., 2020).

Successful drug delivery using NPs would lead to enhanced treatment efficacy, reduced side effects, and better patient adherence to medical treatment.

2.3.2 Theranostics

Metallic and semiconductor NPs have photothermal properties that could be used to improve theranostics systems, since their absorbed light can efficiently be converted into heat that can be turned into selective laser photothermal therapy for diseases like cancer (Chen et al., 2014; Huang et al., 2006; Sztandera et al., 2019).

When these NPs are positioned over the tumour tissue and irradiated with a light source that corresponds to their absorption peak, heat is generated, leading to the destruction of the malignant tissue. However, it is important to avoid damaging the healthy tissue by placing the NPs specifically over the tumour tissue. The most extensively researched materials for this application are Au, which can be tailor the fabrication process to be synthesized in various structures such as spheres, rods, shells, and cages, etc. (Chan, 2007; Huang et al., 2009; Khan et al., 2019).

2.3.3 Biomedical imaging

Imaging techniques like MRI and CT enable the visualization of anatomical structures and some physiological processes. These techniques stand out by their use of imaging probes or contrast agents to enhance the visibility of certain structures, so that more detailed and accurate diagnosis can be provided to patients.

The magnetic properties of NPs have been studied to develop imaging probes and contrast agents that can offer superior image quality compared to current industry-standard contrast agents, while utilizing smaller quantities of material. The tunability of components and dimensions of NPs allow for the precise control of their magnetic properties, furthering the optimization of image quality (Cobley and Xia, 2010).

Iron oxide NPs are widely used for this purpose, either as monometallic or bimetallic with a different metal. Studies have reported that iron is a biodegradable, biologically tolerable, and less toxic material than the heavy metals currently used (Cheong et al., 2011; Kim et al., 2018; Zhou et al., 2014).

2.3.4 Biomolecules monitoring

There has been a growing demand for detecting a wide range of biomolecules with high specificity and low concentrations that keeps motivating the ongoing research on biomolecules monitoring devices. This can be done using a device that is able to transform a biomolecular response into a measurable and analysable signal, also known as sensors. The current trend in the industry aims for smaller devices due to the numerous benefits like easy-to-use products, low-cost mass production, easy storage, and distribution that could lower healthcare costs and enhance the point of care tests for people around the world (Malekzad et al., 2017; Sekretaryova et al., 2016).

However, connecting the biomolecular responses with an electronic device that can quantify and process them remains a challenge for these devices. The use of electrochemistry to do so has been of interest since it would provide a direct conversion to electronic signals. In this case, an electrode would be used to measure the signal, but the performance of the electrode is tightly related to their surface and properties like signal amplification, sensitivity and selectivity towards certain biomolecules can be tailored by modifying the surface of the electrode (Grieshaber et al., 2008; Saha et al., 2012).

This can be achieved by using biocompatible nanomaterials considering that several biomolecules are in the nanoscale already. These nanomaterials could also be tailored to interact with certain biomolecules, enhancing their specificity and selectivity, but also paving the way towards multi-analyte sensor development (Grieshaber et al., 2008).

For this application, metallic NPs made of noble metals like gold, silver, and platinum in different compositions have been studied for their use in biomolecules monitoring. Their previously discusses properties makes them stand out from other metals since they do not only increase the electrode surface area but also increases the sensitivity, selectivity, and repeatability of biomolecule monitoring devices by allowing direct electron transfer and amplifying the acquired signal (Alim et al., 2018; Cobley and Xia, 2010; Jelinek, 2015; Khoshroo et al., 2018; Sekretaryova et al., 2016).

The incorporation of these nanomaterials can be done by attaching them over a sensor's active surface, creating modified electrodes. Numerous studies have focused on modifying electrodes with metallic NPs to monitor biomolecular analytes.

Table 2 summarizes some studies using Au NPs for electrode modification. These studies were not only selected because they study biomolecule monitoring and detection, but also because the electrode modification was done using Au NPs over a carbon-based electrode and used of CV for

electrochemical characterization, which were similar methods to the experimental procedures done in this thesis. Although there are much more studies using similar methods, the chosen studies can demonstrate the potential that Au NPs hold to enhance the monitoring of a wide variety of biomolecules.

Motivated by the risk of overdose on patients that develop a dependence on benzodiazepines, and the costly current techniques for the analysis of this drug. Khoshroo et al. proposed in a research article an electrochemical sensor modified with Ag@Pt NPs supported over graphene nanosheets to measure oxazepam concentrations in samples such as serum, urine, and pills (Khoshroo et al., 2018). The Ag@Pt NPs and graphene nanosheets were synthesized with a chemical method developed by the authors, resulting in an Ag@Pt/Gr nanocomposite that would then be drop casted over the GCE and dried at room temperature. Characterization of the materials was done with SEM, TEM, EIS, and CV.

Glucose sensors are popular among the biosensing industry due to its continuous market growth, increasing the demand for reliable and simple devices to help people keep track of their blood sugar levels effectively (Teymourian et al., 2020).

Miao et al. proposed a study where a glucose biosensor modified with nanocomposite including Au NPs electrodeposited over a GCE in PBS solutions with different glucose concentrations and samples including serum (Miao et al., 2015). The GCE was then immersed in the solution, electrodepositing the Au NPs/PVP/PANI nanocomposite, and then drop casting GOx and letting it dry. The characterization was done using SEM, TEM, and CV.

Kong et al. developed a biosensor using disposable SPCE modified with a nanocomposite including Au NPs coupled with a paper disk to measure glucose levels in PBS solution with different glucose concentrations and blood samples (Kong et al., 2014). The Au NPs/PANI/Gr nanocomposite would be drop casted over the SPCE surface and air dried at room temperature. When the surface is dry, GOx would also be drop casted over the surface and dried. Characterization of the electrode was done with SEM, XPS, Raman spectroscopy, FT-IR, and DPV.

Motivated by developing sensitive biosensors for hematologic disease diagnosis like atransferrinemia, a disease connected to iron deficiency anaemia, liver disease, and certain cancer types, can be fatal if untreated. Rabbani et al. proposed an electrochemical sensor for Tf detection using a GCE modified with Au NPs in PBS solution with different Tf concentrations and in serum (Rabbani et al., 2024). The Au NPs were placed via electroless deposition on top of the GCE surface,

and the surface was then modified further with amino groups of anti-Tf. The electrode was characterized with SEM, XPS, Raman spectroscopy, CV, EIS, and DPV.

Hajihosseini et al. proposed a biosensor using a modified GCE with a nanocomposite including Au NPs for *H. pylori*, since this bacteria is considered a primary cause of gastric cancer (Hajihosseini et al., 2016). GO and Au NPs were drop casted over the GCE and dried at room temperature one at a time, then ssDNA of *H. pylori* would be placed over the surface and incubated for 80 minutes. Characterization of the electrode was done by TEM, SEM, UV-vis, CV, and DPV. The electrochemical measurements were conducted using PBS solution and different concentrations of complementary DNA of the bacteria.

Table 2. Biosensors modified with metallic NPs studies.

Analyte	Electrode	Construction	NPs placement over electrode	Characterization methods
Oxazepam	GCE	Ag@Pt NRs/Gr/GCE	Drop casted	SEM, TEM, CV, and EIS
Glucose	GCE	GOx/AuNPs/PVP/PANI/GCE	Electrodeposited	TEM, SEM, and CV
Glucose	SPCE	GOx/AuNPs/PANI/Gr/SPCE	Drop casted	SEM, XPS, Raman spectroscopy, FT-IR, and DPV.
Tf	GCE	AuNPs/GCE	Electroless deposition	SEM, XPS, Raman spectroscopy, CV, DPV, and EIS
H. pylori	GCE	AuNPs/GO/GCE	Drop casted	TEM, SEM, UV-vis, CV, and DPV

All the previously mentioned studies reported that the results obtained from the characterization measurements with the modified electrodes showed selectivity and sensitivity comparable to existing methods towards their respective analytes. However, the easy set up structure, small analyte volume usage, and low-cost compared to other existing methods can give electrochemical biosensors an advantage in this industry.

3 Electrochemical insights

This chapter provides a short introduction to electrochemistry, describing the components of an electrochemical cell, the roles of the electrodes involved and making an emphasis on the use of GCE. Then, CV will be introduced, along with some applications of this technique.

3.1 Basics of electrochemistry

Electrochemistry is known as a branch of chemistry that studies the relationship between electricity and chemical reactions. Focusing on processes in which chemical energy converts to electrical energy and vice versa, also known as redox (reduction-oxidation) reactions.

An essential part of this science is the electrochemical cell, where electrochemical reactions take place by applying a voltage or current. Starting by placing an analyte in the electrochemical cell as shown in Figure 2, it is a liquid solution that contains the chemical species to be studied. The analyte will interact with the electrodes immersed in the electrochemical cell, resulting in a measurable electrical signal. It is possible to have electrochemical cells with two or three-electrode set ups, yet the latter is preferred due to its improved accuracy. In Figure 2, the typical set up of a three-electrode electrochemical cell is shown, composed of a working electrode (WE), reference electrode (RE), and counter electrode (CE).

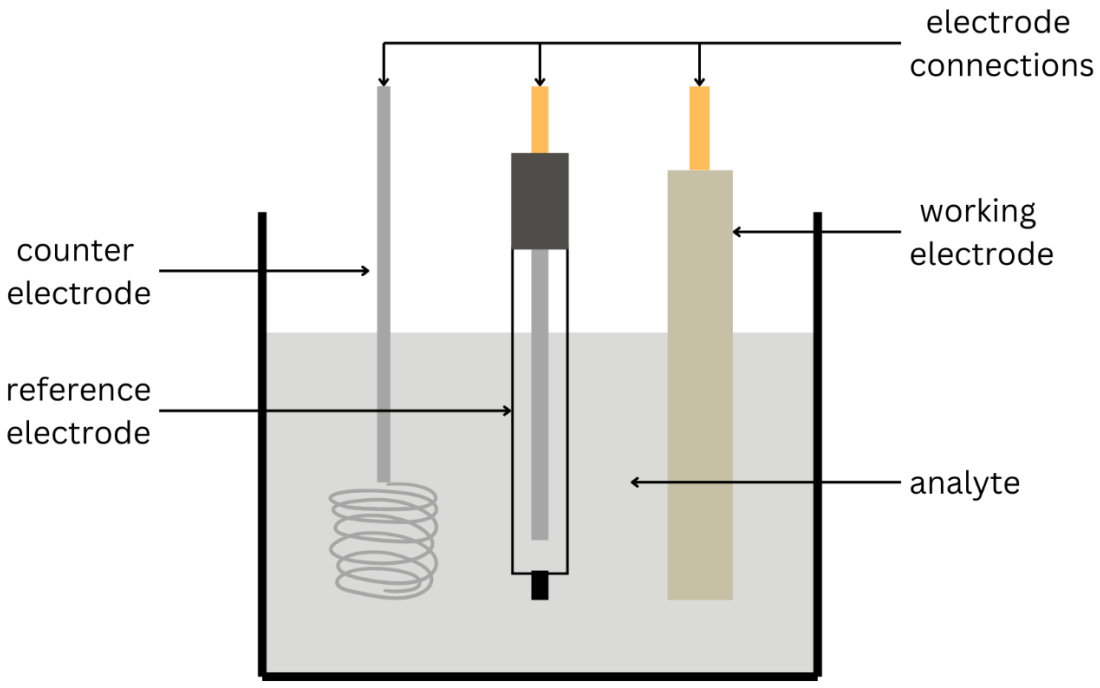

Figure 2. Three-electrode electrochemical cell set up.

The RE, as the name suggests, acts as a reference point to measure how much the potential changed compared to the other electrodes. The potential of the RE is stablished and does not change throughout the measurements.

The electrochemical reaction of interest occurs in the WE, depending on the applied potential, the flow of electrons between the analyte and the electrode will differ. An anodic potential will lead to an oxidation reaction, whilst a cathodic potential will turn into a reduction reaction. There are two conventions used to report electrochemical measurements, US and IUPAC standards. Depending on the chosen convention, potentials may be plotted differently. The US convention, used for this thesis studies, will plot reduction reaction upwards, and oxidation reactions downwards; whilst the IUPAC convention will report it the other way around. Nevertheless, the current that flows through the WE will also go through the CE to balance the current and allow the opposite reaction to take place (Elgrishi et al., 2018; Shanbhag et al., 2023). In the case of the CE, it is recommended to choose an inert material, like platinum (Pt), so that the ongoing reactions are not affected by the material reactivity.

Commonly used RE include SCE and Ag/AgCl. Whilst the WE materials can be more flexible depending on the application, it is desired that the chosen material is inert and has electroconductive properties. Some examples of common WEs are platinum (Pt), gold (Au), and GCE (Espinoza et al., 2019; Grieshaber et al., 2008; Malhotra and Ali, 2018).

One of the most popular electrode types used for electrochemical studies are GCE due to their low-cost, chemical stability, neutral platform, and high electrical conductivity (Elgrishi et al., 2018; Rabbani et al., 2024). However, impurities in the surface of the electrode often result in affected electrochemical measurements. This can be avoided by polishing the surface of the electrode after every measurement.

The previously mentioned electrodes are then connected to a potentiostat, where with a designated software, parameters like scan rate, number of cycles, potential window, etc., can be selected. Depending on the chosen electrochemical technique, certain relevant parameters can be set for it. There are plenty of electrochemical techniques that can be done, yet some of the most popular ones done with a three-electrode electrochemical cell set up are CV, electrochemical impedance spectroscopy (EIS), and differential pulse voltammetry (DPV).

3.2 Cyclic voltammetry

CV is a widely used electrochemical technique that allows the study of the redox process and properties of a chemical species, such as their electrochemical kinetics and reaction mechanisms. In this technique, a voltage window is set, and it will go back and forward between these values at a set speed and for a set number of cycles, recording the current response as the potential is applied in a voltammogram, which can be seen in Figure 3.

The figure below shows a voltammogram, where the x-axis represents the applied potential, and the y-axis represents the measured current. The shapes appreciated in the Figure 3 are often called a "duck" due to its resemblance with the animal, yet the shape is result of the equilibrium described by the Nernst equation (Elgrishi et al., 2018).

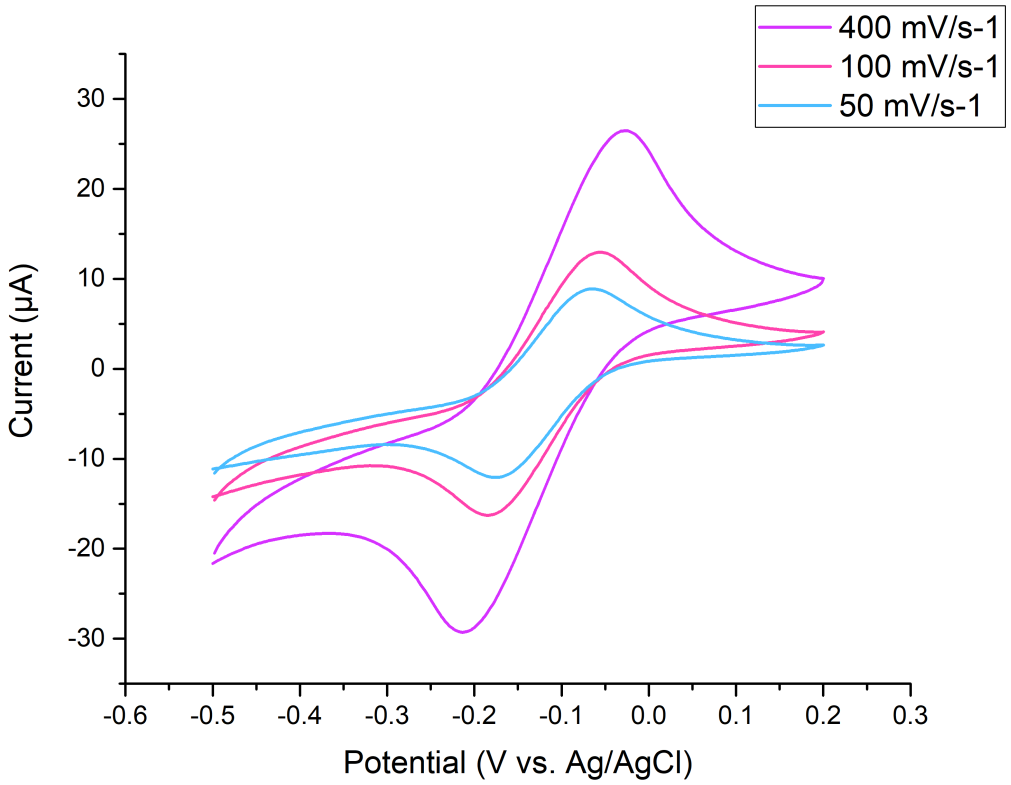

Figure 3. Cyclic voltammogram with different scan rates.

Some important features found in a voltammogram are the peak currents, potentials, and shapes. Peaks can be found because as the applied potential approaches the analyte's reduction potential, the measured current will increase. But once that point has passed and gets closer to the upper limit of the set potential window, the current value will decrease because the oxidation potential has been

exceeded. When the upper potential limit has been reached, the potential will go down to the lower limit, reoxidizing reaction. This reactions will create a peak by increasing and decreasing the current once again but in the negative side of the scale, showing the stability and reversibility of an analyte (Grieshaber et al., 2008).

The set speed is known as the scan rate, expressed as volts per second, it is an important parameter since it determines the speed with which the redox reactions take place. As shown in Figure 3, high scan rates result in high redox reaction speeds, leading to higher measured currents but may tamper with the sensitivity and vice versa.

The shape of a voltammogram will not only depend on the set parameters, but also on the chemical species being studied. Since the concentration of the analyte can impact the height of the peak and different types of analytes will have different park positions (Grieshaber et al., 2008; Malekzad et al., 2017).

The voltammogram shape can also give information about how the electrode interacts with different analytes by looking at the double-layer, surface area, and the adsorption process. CV can also be used to measure the concentration of a chemical species in an analyte. The results obtained from the CV can be interpreted by comparing them to those from conventional methods that measure the same analyte (Shanbhag et al., 2023).

4 Experimental

This chapter describes the methods used to synthesize various types of metallic nanoparticles and the way they were used to understand how the different synthesized nanoparticles affect the electrochemical behaviour of an electrode by placing them on the surface of their active area.

The used chemicals and devices throughout the experiments are mentioned, providing detailed information about the suppliers of the acquired chemicals and the models of the used devices.

Proceeding by describing the synthesis methods used for the various types of metallic nanoparticles, where it is possible to distinguish differences or similarities among them that help tailor the end products. The process of placing the nanoparticles over the electrode's active area is mentioned, followed by describing how the electrochemical studies were set up to assess the electrochemical behaviour of the electrode with the synthesized nanoparticles.

4.1 Chemicals & Apparatus

The chemicals needed for the synthesis of metallic nanoparticles and the relevant electrochemical studies were purchased from Sigma Aldrich, VWR, and Buehler. Hexadecyltrimethylammonium bromide (CTAB), sodium chloride (NaCl), sodium borohydride ($NaBH_4$), polyvinylpyrrolidone (PVP), sulfuric acid (H_2SO_4), benzyldimethylhexadecylammonium chloride (BDAC), gold (III) chloride trihydrate ($HAuCl_4 \bullet 3H_2O$), silver nitrate ($AgNO_3$), l-ascorbic acid (AA), potassium tetrachloroplatinate (II) (K_2PtCl_4), hexaammineruthenium (III) chloride ($[Ru(NH_3)_6]Cl_3$), and sodium phosphate dibasic (Na_2HPO_4) were acquired from Sigma Aldrich. Hydrochloric acid 37% (HCl), nitric acid 68% (HNO_3), sodium hydroxide (NaOH), potassium chloride (KCl), and potassium dihydrogen phosphate (KH_2PO_4) were purchased from VWR. Micro Polish Alumina with 0.05 μm particle size and polycrystalline diamond suspension with 1 μm particle size were purchased from Buehler. All compounds were utilized as received, without any alterations or modifications made to their original form. Solutions were prepared using water purified by reverse osmosis.

Throughout the nanoparticle synthesis, the centrifuge used was a Centrifuge 5810 from Eppendorf. Characterization of the nanorods was done with a UV-vis spectrometer and Transmission Electron Microscope (TEM). The UV-vis spectrometer studies were conducted with the SPECORD 200 PLUS Double-beam spectrophotometer from the company Analytik Jena. While the Transmission Electron Microscopy (TEM) measurements were conducted with a JEM-1400 Plus Transmission Electron Microscope from the company Jeol. Samples were placed on a copper grid for their characterization.

The electrochemical experiments were conducted using the following: a refillable 70 mm Ag/AgCl as RE and a 3mm GCE acting as a WE from Redox.me, and a platinum wire as the CE. The experiments were carried out by a Gamry Reference 620 (potentiostat/galvanostat/ZRA) connected to a Gamry Faraday shield, both from the company Gamry.

4.2 Synthesis methods

The synthesis of metallic nanorods procedures follow a protocol introduced by Vipul Sharma et al. in a research article where a method to fabricate Au NPs with smooth and continuous coatings of platinum (Pt) is developed (Sharma et al., 2016). The methods employed for aspect ratios 3.3 and 2.1 as well as the bone-shaped gold nanorods are novel fabrication procedures.

All required glassware was thoroughly cleaned with aqua regia before the experiment started, reducing the risk of contaminants in the solutions due to the negative impact it would have on the synthesis of the metallic NPs. Aqua regia was prepared fresh when needed, by mixing HCl and HNO_3 forming a 3:1 V/V HCl/HNO_3 ratio. It is vital to mention the importance of adding HNO_3 slowly to the already measured HCl volume, to avoid unwanted reactions.

The solutions were all prepared one day before the experiment, with two exceptions: $AgNO_3$ and $NaBH_4$. $AgNO_3$ solutions were always prepared the same day before starting the experiments, and any glassware containing the solution was covered with aluminium foil to prevent light-induced oxidation. Similarly, $NaBH_4$ solutions were freshly prepared when needed and placed in ice-cold water for at least an hour before the experiments began. Additionally, it is important to note that the $HAuCl_4 \bullet 3H_2O$ chemical and its solutions were always kept in the fridge to avoid degradation due to temperature changes. CTAB and BDAC solutions sometimes needed to be heated until the compounds completely dissolved.

The previously mentioned preparations were applied to all synthesis methods discussed in this chapter.

4.2.1 Different aspect ratio gold nanoparticles

The synthesis of different aspect ratio Au NPs utilizes the non-seeding method. The aspect ratio of the NPs can be tailored as desired by varying the amount and concentration of AA added during the synthesis process, studies have noted that higher amounts and/or concentrations of AA decreases the aspect ratio of NPs (Gou and Murphy, 2005; Jing et al., 2014; Scarabelli et al., 2015). However, it

has been reported that different aspect ratios can also be achieved depending on the amount of $NaBH_4$ added in the synthesis process (Ali et al., 2012).

In this case, spherical Au NPs 3.3 AR and tooth-shaped Au NPs 2.1 AR, were synthesized. The followed process is summarized and shown in Figure 4, it will be described alongside with the differences between the two types of synthesized NPs.

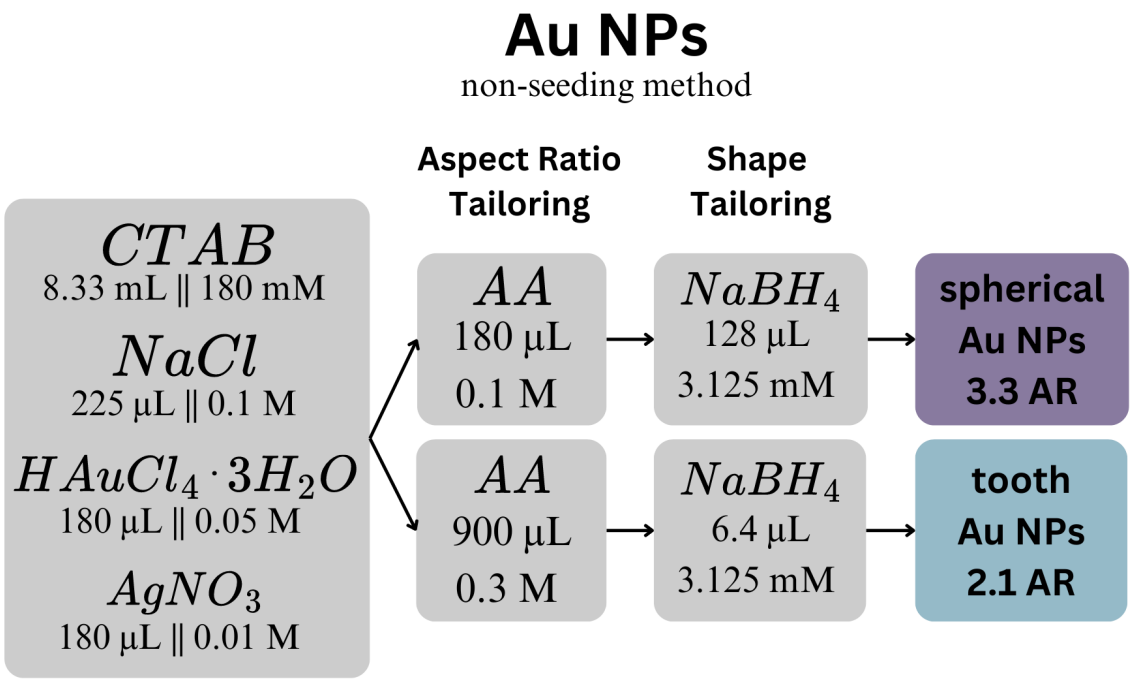

Figure 4. Gold nanoparticles with different aspect ratios and shapes fabrication process infographic.

Both processes initiate by adding 8.33 mL of CTAB with a concentration of 180 mM, alongside 225 µL of NaCl with 0.1 M concentration, 180 µL of $HAuCl_4 \cdot 3H_2O$ with 0.05 M concentration, and 180 µL of $AgNO_3$ with a concentration of 0.01 M to the same vial. After this step, the vial was manually agitated slightly, as the colour of the solution changed from colourless to a yellow-orange tone.

Spherical gold nanoparticles with 3.3 aspect ratio

In this section, the description will follow the route for spherical Au NPs 3.3 AR. Continuing from the last-mentioned step, 180 µL of 0.1 M AA were added to the vial's solution. Followed by closing the vial and shaking it upside down manually for around 30 seconds, as the solution changed from a yellow-orange colour back to colourless.

Then, 128 µL of 3.125 mM $NaBH_4$ were added to the vial by introducing the pipette tip inside the solution. Then the vial was closed securely once again and inverted upside down by hand for around 30 seconds.

Finally, the vials were left at room temperature while the colour change took place. The solution of spherical Au NPs 3.3 AR turned to a deep purple colour with a hint of navy blue, as shown in Figure 5 on the left side. Proper synthesis of spherical Au NPs 3.3 AR was indicated with the colour change of the solution. The NPs were ready to be used and characterized as soon as the colour change takes place.

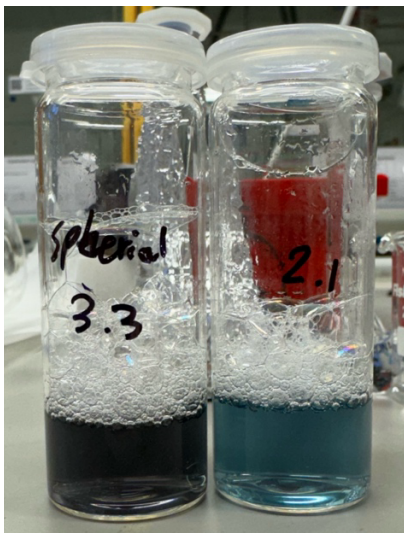

Figure 5. Synthesized spherical Au NPs 3.3 AR & tooth-shaped Au NPs 2.1 AR.

Tooth shaped gold nanoparticles with 2.1 aspect ratio

This section will follow the route to synthesize tooth shaped Au NPs 2.1 AR. After adding all the initial solutions to the vial, 900 µL of AA with a concentration of 0.3 M would be added to the vial. The vial would then be securely closed and shaken upside down manually for around 30 seconds, changing the colour of the solution from a yellow-orange tone to colourless.

Following this, 6.4 µL of 3.125 mM $NaBH_4$ was added to the vial by introducing the pipette tip inside the solution. The vial would be closed once again so it can be shaken manually by inverting the vial upside down for another 30 seconds.

Then, the vials were left alone at room temperature while the colour of the solution changed. In the case of tooth shaped Au NPs 2.1 AR, the solution would acquire a rich electric blue colour like the

shown in Figure 5 on the right side. Colour changing of the solution indicates the proper formation of tooth shaped Au NPs 2.1 AR. The NPs could be used and characterized as soon as the solution's colour changes.

4.2.2 Bone-shaped gold nanorods

Bone-shaped Au NRs were synthesized with a seed-mediated growth method. The process needed a seed solution to be added to a growth solution with reactants that will help the seed solution turn into the desired shape of NRs accordingly, the process is summarized and shown in Figure 6, yet it will be described below.

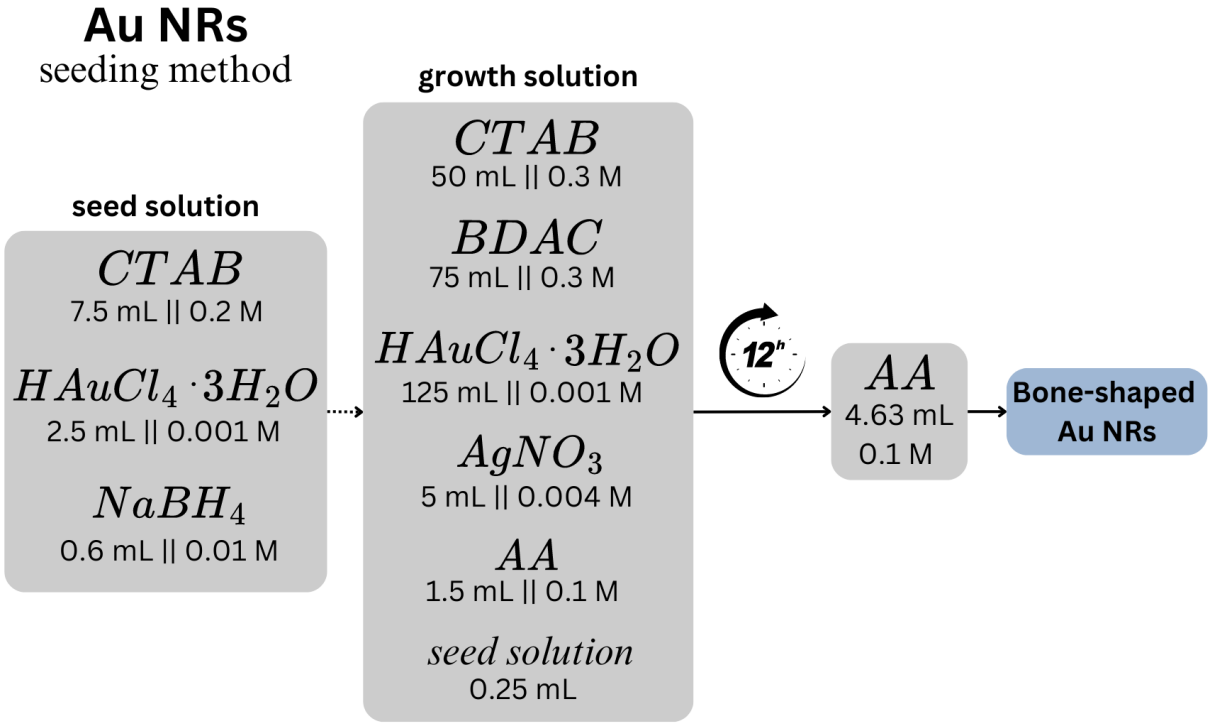

Figure 6. Bone-shaped Au NRs fabrication process infographic.

The experiment begins by preparing the seed solution, this was done by adding 7.5 mL of 0.2 M of CTAB and 2.5 mL of $HAuCl_4 \bullet 3H_2O$ with a concentration of 0.001 M in a vial. Following this step, the vial was manually stirred for a few seconds. Then 0.6 mL of 0.01 M $NaBH_4$ was added to the same vial. Upon the completion of this step, the vial would be closed and gently agitated by hand for around 2 minutes, the colour of the solution would change to a dark yellow tone as seen in Figure 7. With the conclusion of this step, the vial was left undisturbed for half-hour at room temperature; once the time has passed, the solution can be used to undergo the following steps. However, the seed

solution was to be used within 2 to 3 hours once the seed solution completion due to the aging of the reagents; the solution's colour changes to white as it ages.

Figure 7. Seed solution for seeding method for synthesis of bone-shaped Au NRs.

After the seed solution is prepared, the synthesis continues with the preparation of the growth solution. In a glass container, 50 mL of CTAB with a concentration of 0.3 M, alongside with 75 mL of BDAC with a concentration of 0.3 M, and 125 mL of 0.001 M $HAuCl_4 \bullet 3H_2O$ were added. Mixing these solutions together turned the solution to a dark orange colour as shown in Figure 8a.

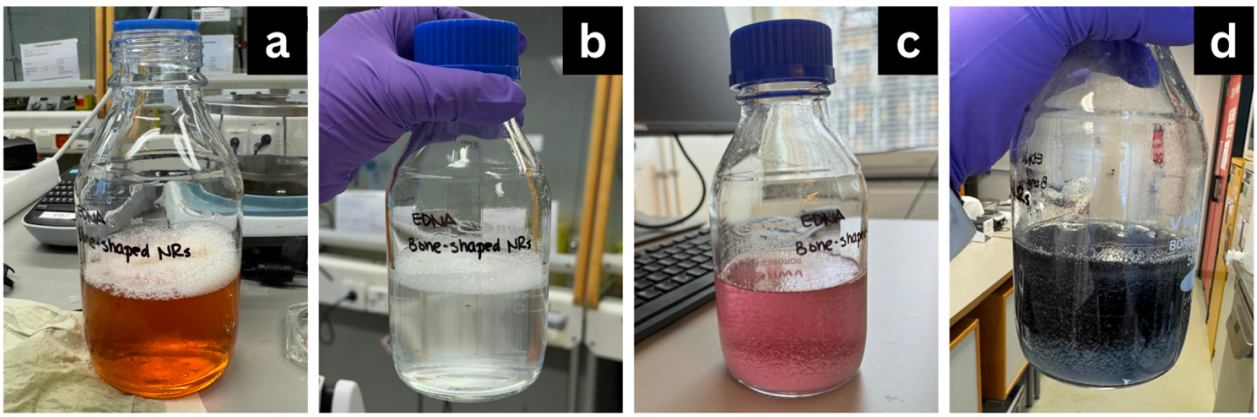

Figure 8. Growth solution for seeding method for synthesis of bone-shaped Au NRs. a) Growth solution colour change to dark orange, b) Growth solution colour after adding seed solution, c) Growth solution colour change after being left overnight, and d) Bone-shaped Au NRs solution 3 hours after AA addition.

Following this step, 5 mL of $AgNO_3$ with a concentration of 0.004 M was added to the glass container and then it was swirled gently manually for a few seconds. Then 1.5 mL of AA with a concentration of 0.1 M were added to the solution. Upon the addition of AA, the container was closed securely and

gently shaken upside down manually until the colour of the solution changed from dark orange to colourless, as shown in the Figure 8b.

Once the colour change has occurred, 0.25 mL of the previously prepared seed solution was added to the container by submerging the pipette tip in the solution to do so. Then the solution was kept undisturbed at room temperature overnight.

There was no immediate colour change in the solution after the addition of the seed solution, but the next day, the solution's colour changed from colourless to a deep purple-pink colour, as seen in the Figure 8c.

That same day, 4.63 mL of AA with a concentration of 0.1 M were added to the glass container with the solution that was left overnight and twirled gently for a few seconds by hand. The solution was then left undisturbed for around 3 hours at room temperature, in which the solution's colour changed from a deep purple pink to a deep blue colour as seen in the Figure 8d.

This colour change indicated the successful synthesis of bone-shaped Au NRs. As soon as the colour changes, the bone-shaped Au NRs were ready to be characterized and used for further experiments.

4.2.3 Capsule-shaped gold core with platinum shell nanorods

The synthesis of capsule-shaped Au@Pt NRs was conducted in steps. Starting by capsule-shaped Au NRs, followed by turning them into capsule-shaped Au@Ag NRs. Once this step was reached, two types of capsule-shaped Au@Pt NRs were synthesized: Au@Pt-DC NRs and Au@Pt-C NRs.

Capsule-shaped gold nanorods

The non-seeding method was implemented in the synthesis of capsule-shaped Au NRs. This is the first step in the synthesis of capsule-shaped Au@Pt NRs.

Figure 9 shows a quick overview of the capsule-shaped Au NRs. However, the synthesis begins by adding 8.33 mL of CTAB with a concentration of 180 mM, 225 μL of 0.1 M NaCl, 180 μL of $HAuCl_4 \bullet 3H_2O$ at 0.05 M concentration, and 180 μL of 0.01 M $AgNO_3$. Following this, the vial would be twirled manually by hand for a few seconds as the colour of the solution changed from colourless to a yellow-orange tone.

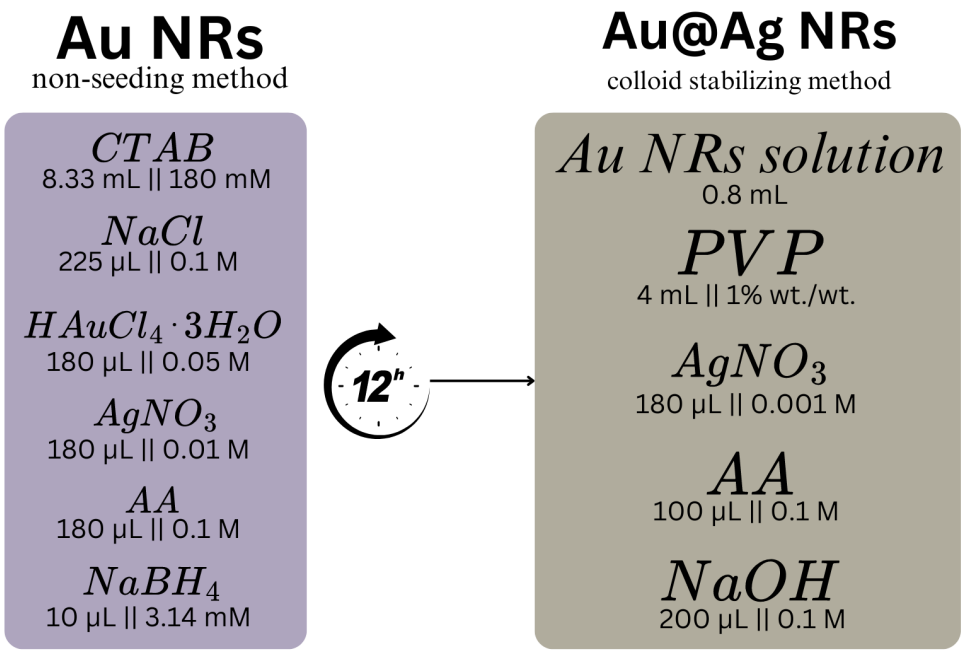

Figure 9. Capsule-shaped Au NRs and Au@Ag NRs fabrication process infographic.

As soon as the colour of the solution has changed, 180 µL of AA with a 0.1 M concentration were added to the solution. The vial would then be closed securely to be inverted up and down gently by hand for around 30 seconds, during this time the colour of the solution would change from a yellow-orange tone back to colourless.

Then 10 µL of $NaBH_4$ at 3.14 mM concentration were added to the vial by submerging the pipette tip inside the solution. After the addition of $NaBH_4$, the container was closed and shaken gently upside down manually for around 30 seconds. The solution was then left undisturbed at room temperature overnight. At first, the solution would remain colourless, but with time the colour started to go through various shades of purple until it reaches a dark purple tone, as shown on Figure 10.

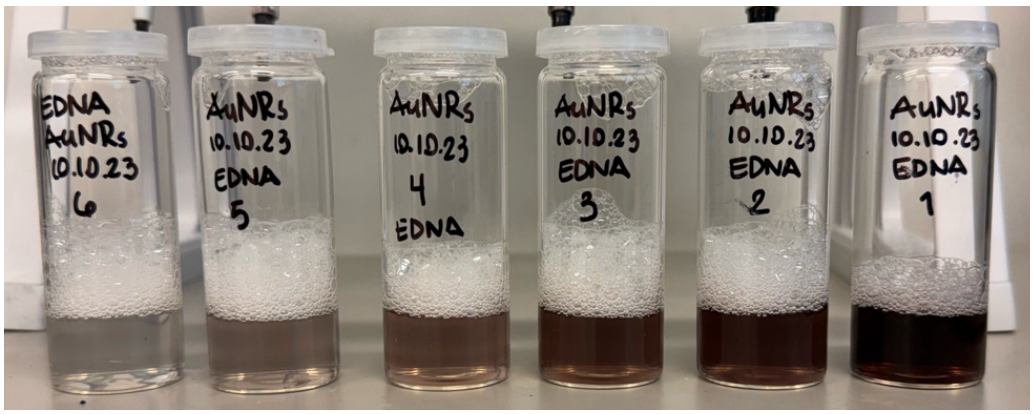

Figure 10. Transformation of capsule-shaped Au NRs colour solution over time.

The colour change to dark purple indicates the successful synthesis of capsule-shaped Au NRs. However, for them to be characterized or used in the next steps of the fabrication process the synthesized capsule-shaped Au NRs had to be purified through centrifugation. The solutions were transferred to centrifuge tubes and the remaining solution of the vials was washed with minimal amounts of water. The final volume in the centrifuge tubes was always kept at 15 mL to avoid tampering the concentration of the solution by adding too much water.

Centrifugation was done in at least four periods of 10 minutes with a speed of 8,500 rpm. This was repeated as many times needed until the CTAB was no longer seen in the bottom of the tube.

It is important to highlight the importance of purifying the capsule-shaped Au NRs close to when the NRs are meant to be used or characterized since by purifying them early on can cause them to clump together and may affect the experimental results.

Capsule-shaped gold core with silver shell nanorods

The synthesis of capsule-shaped Au@Ag NRs was carried out with a colloid stabilizing method with PVP. This is the second step in the synthesis of capsule-shaped Au@Pt NRs, since the similarity of lattice structures between silver (Ag) and gold (Au) forms a uniform coating over the other metal's surface.

An overview of the capsule-shaped Au@Ag NRs synthesis process was summarized and shown in Figure 9.

The first step involves adding 4 mL of 1% wt./wt. of PVP and 0.8 mL of the previously synthesized and purified capsule-shaped Au NRs to an unused vial. Once this was done, the vial was slightly agitated manually for a few seconds.

Following this, 180 μL of $AgNO_3$ with a concentration of 0.001 M and 100 μL of AA at 0.1 M concentration were added to the solution. The vial would then be lightly agitated by hand again for a few seconds.

Then, 200 μL of NaOH at 0.1 M concentration were added to the solution and then manually agitated for a few seconds. The colour of the solution changed to a turquoise blue-dark green tone, shown in Figure 11, the change may occur either immediately or may take a few seconds to do so.

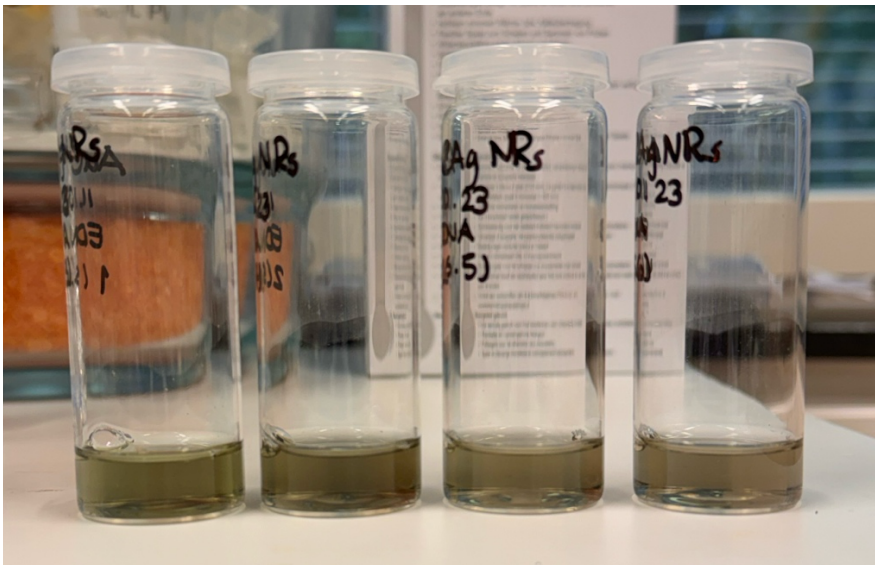

Figure 11. Capsule-shaped Au@Ag NRs.

The successful synthesis of capsule-shaped Au@Ag NRs would be indicated with the colour change. The NRs could be characterized and used for further experiments as soon as the colour change occurred.

Capsule-shaped gold core with discontinuous platinum shell nanorods

Galvanic replacement of silver (Ag) was utilized to synthesise capsule-shaped Au@Pt-DC NRs. However, the shell can be tailored as desired; in Figure 12 an overview of the synthesis process for capsule-shaped Au@Pt NRs is shown. In this case, the first process to be described is the one to synthesize capsule-shaped Au@Pt-DC NRs.

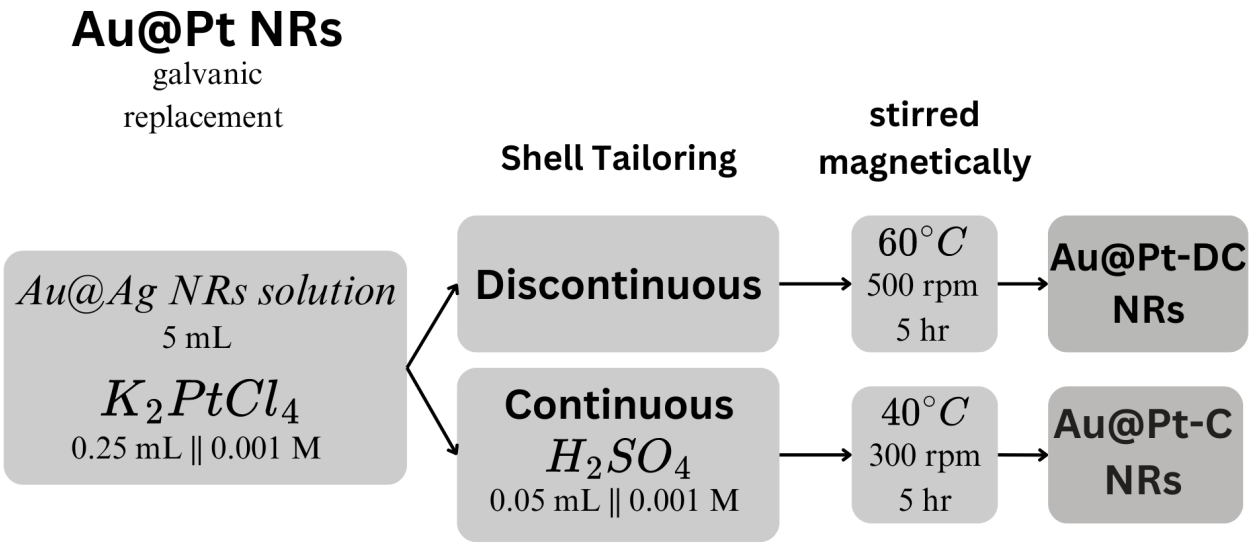

Figure 12. Capsule-shaped Au@Pt NRs fabrication process infographic.

Starting by adding 5 mL of the previously synthesized capsule-shaped Au@Ag NRs and 250 µL of K_2PtCl_4 with a concentration of 0.001 M to a vial.

Once the solutions are added, the solution was then magnetically stirred for 5 hours with a speed of 500 rpm and set to a temperature of 60 ºC. At first, the colour of the solution would change from the previous light blue-dark green colour to a light grey tone but once the magnetic stirring process finishes, the solution would take a darker grey tone as the one seen on the left side of Figure 13.

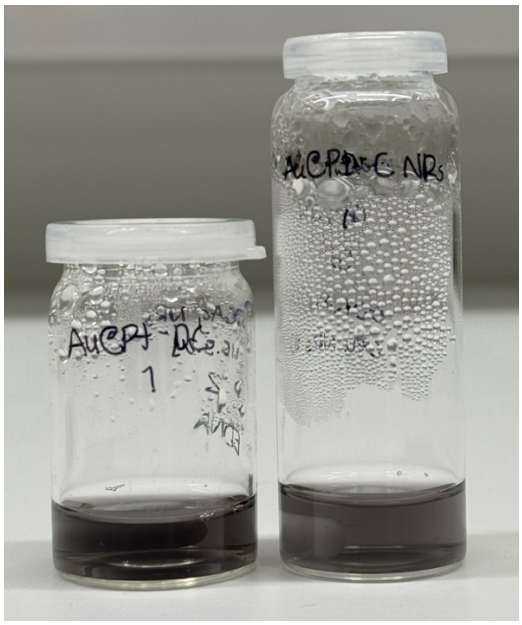

Figure 13. Capsule-shaped Au@Pt NRs. Left vial, capsule-shaped Au@Pt-DC NRs. Right vial, capsule-shaped Au@Pt-C NRs.

The colour change indicated the successful synthesis of capsule-shaped Au@Pt-DC NRs. However, to be used for further experiments and characterized, the solution was centrifuged to collect and purify the NRs from surfactants.

The solutions were transferred to centrifuge tubes, and the vial was rinsed with minimal amounts of water to collect any remaining solution. Centrifugation was done one time only, set with a speed of 7,000 rpm for 20 minutes.

It is important to stress that the capsule-shaped Au@Pt-DC NRs should be purified close to when they are to be used or characterized. This will avoid them to clump all together and potentially hinder the experimental results.

Capsule-shaped gold core with continuous platinum shell nanorods

The synthesis of capsule-shaped Au@Pt-C NRs was conducted utilizing galvanic replacement of silver (Ag) in presence of H_2SO_4. Using bisulphate adsorption and galvanic replacement to selectively block the platinum (Pt) surface helps to achieve a continuous surface. Now, the synthesis process for capsule-shaped Au@Pt-C NRs shown in Figure 12 will be described.

Synthesizing this type of NRs is highly similar to the one mentioned before. The process starts by adding 5 mL of previously synthesized capsule-shaped Au@Ag NRs solution and 250 μL of K_2PtCl_4 at 0.001 M concentration into a vial. Yet, in this case, 50 μL of H_2SO_4 with a concentration of 0.02 M is also added to the solution.

The solution was also magnetically stirred for 5 hours but with different settings, the speed was set to 300 rpm, and the temperature to 40 ºC. The colour of the solution also changed from the turquoise blue-dark green tone to a light grey one that would intensify when the magnetic stirring time ends, the solution would end up looking like the one seen on the right side of Figure 13.

When the colour of the solution changes place, it indicates that capsule-shaped Au@Pt-C NRs have been synthesized. Yet, it was necessary to centrifuge them to collect and purify the NRs so they could be used for further experiments and characterized.

The solutions were moved to centrifuge tubes, and the residual contents from the vial were washed with minimal amounts of water. Centrifugation was done for 20 minutes one time only and the set speed was 7,000 rpm.

The centrifugation of the capsule-shaped Au@Pt-C NRs should be done close to when they will be either used or characterized. This is advised to prevent them to clump together and potentially affecting the experimental results.

4.3 Electrochemical studies

To understand how different NPs and nanorods NRs affect the electrochemical behaviour of a GCE, the electrode would first be polished thoroughly, making sure there are no contaminants over the active surface. Followed by drop casting 5 μL of a synthesized nanomaterial on the active surface of the GCE and letting it evaporate at room temperature in an area where light does not hit the electrode directly, this would take around an hour to do so. Once the experiment is set up, the cyclic voltammetry measurements would be conducted, and the electrode was polished once again to avoid

cross-contamination from analytes and materials. This would be repeated for all the synthesized NPs and NRs mentioned below.

The synthesized NPs and NRs that were used for the following electrochemical studies were: spherical Au NPs 3.3 AR, tooth-shaped Au NPs 2.1 AR, bone-shaped Au NRs, capsule-shaped Au@Pt-DC NRs, and capsule-shaped Au@Pt-C NRs.

Every time the GCE was to be polished, it would be done with 0.05 μm Micro Polish alumina and/or 1 μm polycrystalline diamond suspension to ensure the proper removal of any contaminants in the surface. The electrode would be polished doing a figure-eight motion over a polishing pad with one of the previously mentioned materials on top. This was done to avoid uneven polishing that circular or linear motions may cause. The electrode was polished until no contaminants could be seen on top of the active surface.

Both RE and CE were thoroughly rinsed with water after every measurement to avoid cross contamination in between experiments.

4.3.1 Potential windows

PBS solution was prepared by dissolving 80 g of NaCl, 2.0 g of KCl, 14.4 g of Na_2HPO_4, and 2.4 g of KH_2PO_4 into 1 L of deionized water. Once all the chemicals are well incorporated, the pH of the solution should be 6.8. However, in case the pH differs it can be adjusted by adding NaOH or HCl to the solution. Then, the 1 L of PBS solution would be diluted with 9 L of deionized water. Resulting in 10 L of PBS solution with a final pH of 7.4.

The experiment set up starts by adding 50 mL of PBS solution to a glass cell. Then, the electrodes would be placed inside the glass cell with their respective connections to the potentiostat, as shown in Figure 2.

The settings for the cyclic voltammetry experiments were set to run for 3 cycles with a scan rate of 50. However, the set potential window would broaden between measurements depending on the current value achieved in that round.

At first, the potential window was set to 0.4 – 0.6 V to be almost in the centre of the scale, and then that window would keep opening by +/- 0.1 V per side until a measured current value peak goes slightly over the 1 μA mark on their positive and/or negative side.

4.3.2 Outer sphere redox probe studies

The $[Ru(NH_3)_6]Cl_3$ with KCl as buffer solution was always prepared fresh to avoid degradation due to temperature changes. Starting by preparing 1 M of KCl, followed by adding 1 mM of $[Ru(NH_3)_6]Cl_3$ to it and allowing them to incorporate well before placing it in the fridge.

The chemical $[Ru(NH_3)_6]Cl_3$ should be always kept in the fridge to avoid degradation caused by time and temperature difference. Failing to do so may affect the chemical's quality when used for experiments. However, when electrochemical experiments take place, it is important to make sure the prepared solution is at room temperature to avoid measurement irregularities and damaging the electrodes due to the low temperatures.

The experimental setup begins by adding 50 mL of the previously prepared solution of 1 mM of $[Ru(NH_3)_6]Cl_3$ and 1 M KCl to a glass cell, the electrodes were then set up as shown in Figure 2.

Followed by setting the cyclic voltammetry parameters, the experiment would run for 3 cycles, the voltage window was set between -0.5 V to 0.2 V. The measurements were done with three different scan rates: 400 mV/s^{-1}, 100 mV/s^{-1}, and 50 mV/s^{-1}.

5 Results & Discussion

The thesis work focused on fabricating various metallic nanoparticles, aiming to control their size, shape, and composition. This chapter will discuss the characterization of the synthesized metallic NPs and NRs, alongside with the study of their electrochemical behaviour when placed on an electrode using PBS solution and $[Ru(NH_3)_6]Cl_3]$ with KCl as buffer as analytes.

TEM and UV-Vis spectroscopy were used to characterize the nanoparticles' structure, size, and surface. On the other hand, CV was used to define the potential window and outer sphere redox probe behaviour.

The work presented in this thesis has the potential to expand. by studying how the placement of the synthesized NPs affects the electrochemical response of an electrode. Comparing it to the random distribution achieved when the nanomaterial is drop casted on the electrode's surface. At the same time, the electrode could be tested in different analytes containing biomolecules, so that their potential as biomolecule monitoring devices can be studied further.

5.1 Nanoparticles characterization

To characterize the various types of synthesized metallic NPs, techniques like UV-Vis spectroscopy and TEM were utilized, as these imaging methods were complimentary to each other.

The synthesis of the NPs and NRs was first determined from the UV-Vis absorption spectrum since this device can measure optical absorption, transmittance, reflectance, and detect the presence of byproducts in the solution (Khan et al., 2019). Considering the metallic composition of the synthesized nanomaterials and their previously introduced optical properties, UV-visible spectroscopy was a suitable characterization method for them. This technique would be used first to have an overall idea of the quality of the synthesized materials, since impurities or unwanted synthesized nanostructures would affect the measured spectrum.

TEM was then used to characterize the synthesized nanomaterials, since this technique is known for allowing to determine the size, shape, composition and structure of nanomaterials (Scarabelli et al., 2015; St. Angelo, 2014). Considering that using TEM allows obtaining pictures of samples with different magnifications that can provide plenty information of their size, structure, and visualize the presence of byproducts; this imaging technique was considered appropriate to characterize the various metallic NPs.

To visualize and understand the ongoing changes throughout the synthesis process, the following materials were characterized: Au NPs 3.3 AR, Au NPs 2.1 AR, bone-shaped Au NRs, capsule-shaped Au NRs, Au@Ag NRs, Au@Pt-DC NRs, and Au@Pt-C NRs. These materials were classified based on their primary metallic component, gold (Au), and whether they were utilized in the fabrication process of Au@Pt NRs.

5.1.1 UV-visible spectroscopy

By analysing the UV-Vis absorption spectrum using deionized water as reference, the synthesis of various metallic NPs could be determined, alongside with the presence of impurities in the NPs solutions.

The wavelength range was set to run from 400 to 1,100 nm for all the materials mentioned above. However, for the UV-Vis absorption characterisation of the bone-shaped Au NRs, the wider wavelength range was needed but limited due to the device availability.

To visualize the difference among the synthesized NPs, Au Ps were also characterized using 0.05 M $HAuCl_4 \bullet 3H_2O$ solution, the one used in the experiments.

Gold nanoparticles

In Figure 14, the UV-Vis absorption spectrum of Au Ps, spherical Au NPs 3.3 AR, tooth-shaped Au NPs 2.1 AR, and bone-shaped Au NRs is shown. All the spectrums showed a similar slight rise in their absorption between 830 to 838 nm that can be seen on the figure below.

The $HAuCl_4 \bullet 3H_2O$ solution had a yellow colour when characterized, looking at the spectra measurement seen in the figure below, there are no peaks that stand out but a significant decrease instead. The spectrum started in an absorption of 0.582, yet from 459 nm onwards there was a steep fall until 545 nm where the absorption reached a value of 0.0198. After the latter wavelength was reached, the spectra remained constant from that point on.

Moving on to the spherical Au NPs 3.3 AR, this solution showed a deep purple colour with a hint of navy blue like the one seen in the left side of Figure 5. Different from the Au Ps spectra, the measurement of the spherical Au NPs 3.3 AR started at an absorption value of 0.67 and had two peaks at 508 and 520 nm. Then the absorption levels begin to drop from wavelength 618 nm onwards, yet the values do not drop as drastically nor remain constant as the one seen on Au Ps.

The tooth-shaped Au NPs 2.1 AR solution had the same rich electric blue colour as the one seen in the right side of Figure 5. This spectrum had a slightly similar behaviour to the one of the spherical Au NPs 3.3 AR, since it also shows the two peaks at 508 and 520 nm and has a drop on its absorption levels as well. However, the measurement starts at a higher absorption value of 0.7107 and after the two peaks there is a slight drop on the absorption levels. These values would have a more significant and constant fall once the 770 nm wavelength was reached.

The last material shown in Figure 14 are bone-shaped Au NRs, this solution had a deep blue colour as the one seen in Figure 8d. Different from the other materials mentioned before, this spectrum showed 2 significant peaks, one at 608 nm and the second one at 1097 nm wavelength. The absorption level started at 0.5804, close to the one seen on Au Ps spectrum. Yet, the bone-shaped Au NRs absorption level showed a slight drop until 480 nm, where it then rises until the first peak is reached. Once here, the level falls once again until 764 nm wavelength is reached, where the level rises to reach its second peak.

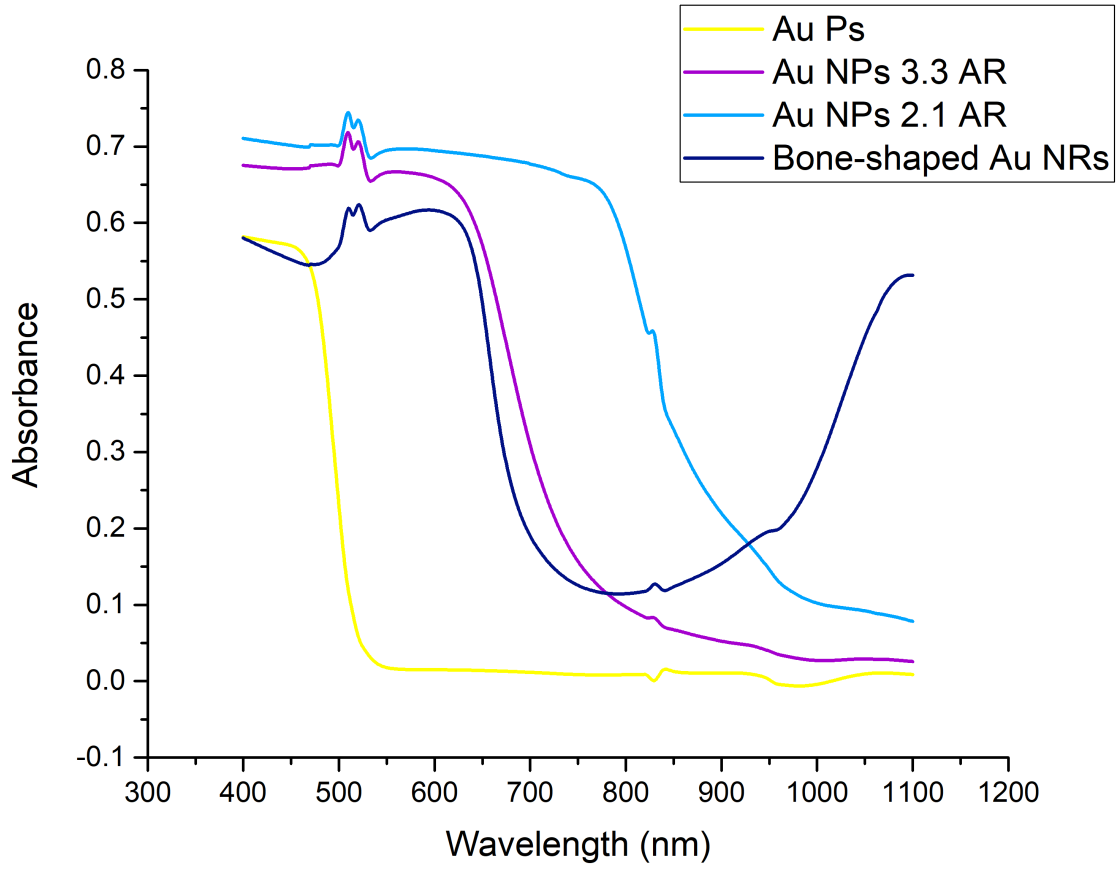

Figure 14. UV-Vis absorption spectra of gold particles (Au Ps), tooth shaped gold nanoparticles with 2.1 aspect ratio (2.1 AR Au NPs), spherical gold nanoparticles with 3.3 aspect ratio (3.3 AR Au NPs), and bone-shaped gold nanorods (Au NRs).

Looking at the different peaks and absorption spectra among these materials are in Figure 14, it is safe to say that the material compositions have changed from the one seen in its metal precursor. The absorption difference is related to the concentration and size of the material; smaller Au nanostructures have reported higher absorption rates than bigger ones in several studies (Burda et al., 2005; Njoki et al., 2007). The TEM characterization would confirm that the spherical Au NPs 3.3 AR and the tooth-shaped Au NPs 2.1 AR had the more uniform and smaller sizes compared to the other materials seen in Figure 14.

The addition of other compounds in the solution for the synthesis process affected the measured absorption spectra. This can be seen with Au Ps and spherical Au NPs 3.3 AR, where even though both have spherical looking shapes, the size difference, shape homogeneity and addition of other compounds to synthesize the spherical Au NPs 3.3 AR changed the measured spectrum among them as shown in Figure 14. This can also be seen with the tooth-shaped Au NPs 2.1 AR and bone-shaped Au NRs, since their shape and size makes light hit them it a different way than it would hit a spherical structure.

The small bumps throughout the spectra can show the presence of small impurities from the added compounds, glassware, or synthesis of different nanostructures in the solution.

Capsule-shaped gold core with platinum nanorods

In Figure 15, the UV-Vis absorption spectrum of Au Ps and capsule-shaped Au NRs, Au@Ag NRs, Au@Pt-DC NRs, and Au@Pt-C NRs is shown. These were the steps followed in the experiments to synthesize Au@Pt NRs. All the spectrums showed two similar peaks on their first significant peak at 512 nm and 524 nm, with another similar slight rise between 830 to 831 nm that can be seen on the figure below.

The $HAuCl_4 \bullet 3H_2O$ solution had a yellow colour when characterized. The figure below shows that instead of a prominent peak, a notable decrease was observed. The spectrum initially displayed an absorption of 0.582, but from 459 onwards there was a sharp decline until 545 nm, where the absorption dropped to 0.0198. Beyond this wavelength, the spectrum absorption level remained constant. was also characterized to visualize the changes in each step.

Au NRs were synthesized on the first step, the solution had acquired a dark purple colour as seen in Figure 10. This spectrum is characterized by having two significant peaks, one at 512 nm and the other at 705 nm, where their absorption reached values of 0.524 and 0.617 respectively. At first, this spectrum had an absorption of 0.476, it had some drops before reaching the significant peaks. Once

the second significant peak was reached, the absorption remained constant until it showed a progressive decrease from the 815 nm wavelength onwards.

Moving to the second step, the capsule-shaped Au@Ag NRs, which had acquired a turquoise blue-dark green colour. This spectrum would start at a 0.2734 absorption value, where then two significant peaks would be seen at 512 nm and 670 nm with absorption values of 0.250 and 0.468 respectively. Just as the spectrum of Au NRs, there would be depressions right before a significant peak would be reached. Yet these two differ because the spectrum of Au@Ag NRs decreases progressively right after the second significant peak is reached, it does not stay constant for a while like the one in Au NRs.

The capsule-shaped Au@Pt-DC NRs solution had dark grey colour. Starting with an absorption of 0.417, there is an overall slight drop in this value throughout the spectrum. However, there are two significant peaks, one at 512 nm and another one at 831 nm. After the second peak the absorption levels decrease in controlled manner and then drop further in a different way after the wavelength reaches the 965 nm mark. This spectrum is not like the ones observed in previously mentioned materials since there are not pronounced peaks, but this spectrum does exhibit some minor peaks.

Finally, the solution containing capsule-shaped Au@Pt-C NRs had also a dark grey colour but slightly lighter than the ones from Au@Pt-DC NRs, just as shown on Figure 13. The spectrum showed a similar behaviour to the one from Au@Pt-DC NRs, with slight significant peaks at 512 nm and 831 nm. However, the absorbance started at 0.344 and would experience a slightly yet remarkable depression around 660 nm wavelength. What stands out the most of this spectrum and the one from Au@Pt-DC NRs is that after the second significant peak, both absorption spectrums follow almost the same path.

The absorption levels and peak distribution differ among all the materials shown in Figure 15, confirming that the different steps in the synthesis process did affect the size and composition of the nanomaterials. As it was explained on the previous category, smaller nanostructures show higher absorption levels, which are seen with Au Ps and capsule-shaped Au NRs. This was confirmed with the TEM images in the following section.

The core@shell NRs were the biggest ones visualized in Figure 15. The effect of shells over Au NRs on the UV-vis absorption spectra has been studied and reported in several studies (Srnová-Šloufová et al., 2004; Toshima and Yonezawa, 1998).

The capsule-shaped Au@Ag NRs, the second step of the synthesis process, had the lowest absorption level and had slight shift in their peaks; meaning they were the biggest material in this category. This was caused due to the thick silver shell that was confirmed in the TEM image in Figure 21 that affects the position of the peak. At the same time, the peak shift has been reported to be correlated to the thickness of the silver layer in the nanostructure, since it affects the measured spectrum due to the difference in the dielectric function between gold and silver (Liu and Guyot-Sionnest, 2004).

On the other hand, the capsule-shaped Au@Pt NRs had an interesting result. Starting with the different absorption level, meaning that the size among the Au@Pt-DC and Au@Pt-C NRs differs. The Au@Pt-DC NRs behaviour has been studied on different research articles, in which the dielectric factor between these metals is explained to be an important factor behind the discontinuous shell distribution and size difference (Guo et al., 2007; Srnová-Šloufová et al., 2004). Whilst Au@Pt-C NRs appear to have a slightly bigger size than Au@Pt-DC NRs, this could be due to the coating of platinum (Pt) that may have synthesized as a thick shell over the Au NRs.

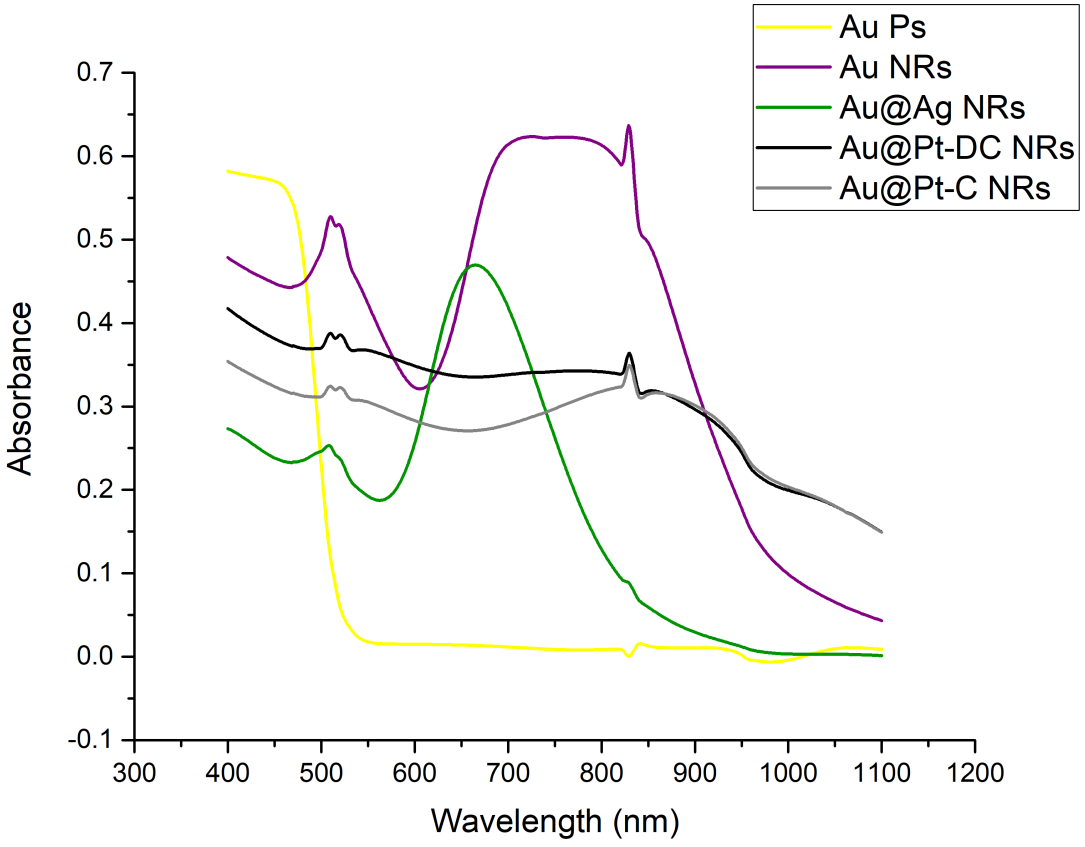

Figure 15. UV-Vis absorption spectra of Au Ps and capsule-shaped Au NRs, Au@Ag NRs, Au@Pt-DC NRs, and Au@Pt-C.

5.1.2 Transmission electron microscopy

TEM is an imaging technique in which a beam of electrons is transmitted through an ultra-thin specimen and as the electrons go through, they interact with atoms in the sample, forming a high-resolution image of it. When used for nanomaterial characterization, TEM images can provide detailed information of the size, shape, and composition of the nanostructure, making it an ideal imaging method for analysing various metallic NPs.

As it was mentioned in the synthesis methods, all synthesized nanomaterials were purified from surfactants through centrifugation prior to their characterization. The samples would then be prepared for TEM characterization by placing a drop of the synthesized nanomaterial solution on a copper (Cu) grid and dried at room temperature before it was introduced into the microscope. In some cases, the concentration of the nanomaterial solution would be too high, and it would not let the electrons pass through the sample. This was solved by diluting the solution by a factor of 10.

The description of the synthesized nanomaterials TEM characterization will follow the order of appearance from the synthesis methods sections.

Considering that the main metal used in the nanomaterial synthesis is gold, $HAuCl_4 \bullet 3H_2O$ solution with 0.05 M concentration, was also characterized so that the changes within the fabricated nanomaterials could be easily appreciated.

In Figure 16 Au Ps from the $HAuCl_4 \bullet 3H_2O$ solution are be observed. As it can be appreciated, there are plenty of Au Ps in different sizes, majority of which have a circular shape, while some have an oval-like shape.

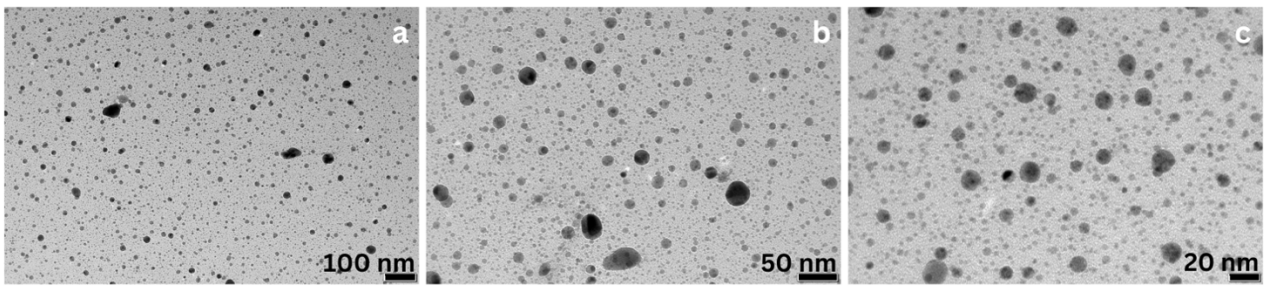

Figure 16. TEM Images of Au Ps.

Gold nanoparticles

On Figure 17, the spherical Au NPs 3.3 AR can be observed. These nanoparticles were described as “spherical” due to the shapes that are shown in the figure below, which are much rounder and defined

shape than the ones of Au Ps in Figure 16. At the same time, the size seen in the spherical Au NPs 3.3 AR is much more uniform than the one seen on Au PS.

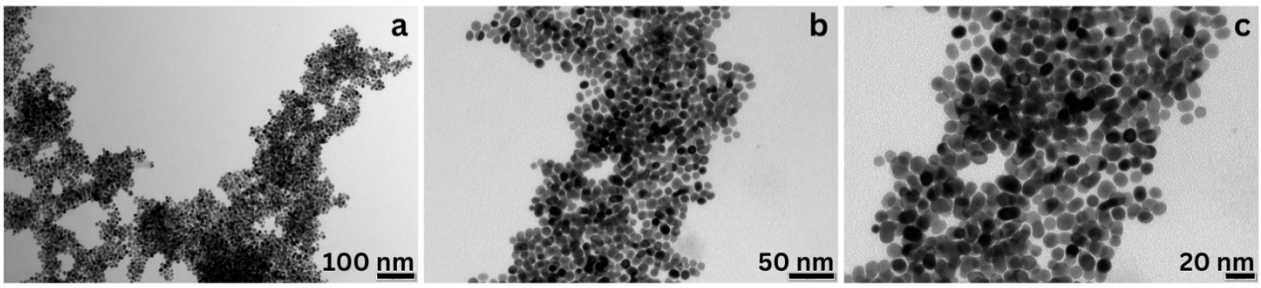

Figure 17. TEM Images of spherical Au NPs 3.3 AR.

The tooth-shaped Au NPs 2.1 AR are shown on Figure 18. Their "tooth-shaped" name was chosen due to the human tooth-like structure that was seen when the TEM characterization took place. This type of NPs has more of a defined rectangular shape, yet it has round edges and irregularities throughout the structure. When compared to the materials in Figure 16 and 17, the shape and size differs highly. The tooth-shaped Au NPs 2.1 AR are not only bigger than the Au Ps and spherical Au NPs 3.3 AR, but the shape is more defined than the one of Au Ps and is more rectangular than the spherical NPs.

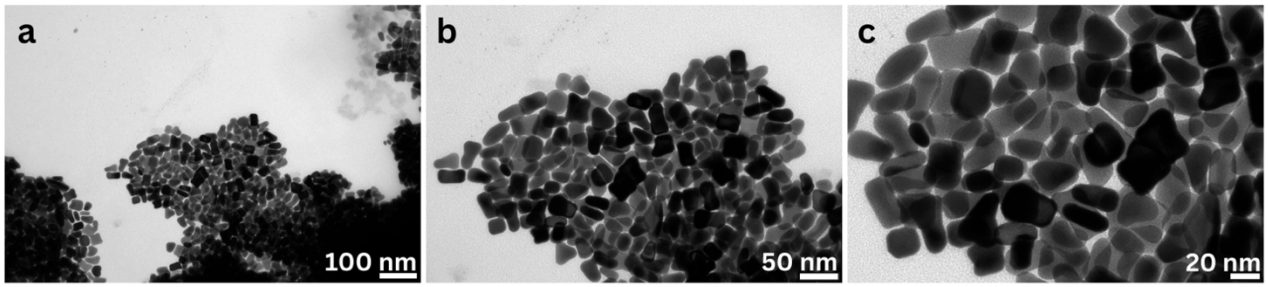

Figure 18. TEM Images of tooth-shaped Au NPs 2.1 AR.

Bone-shaped Au NRs are shown in Figure 18, this name comes from their resemblance with a human bone structure. The reason behind this is their accentuated corners, which is a result of the extra addition of AA during the synthesis process described before. The corners can be more accentuated if desired by repeating the addition of AA on the final step a day later due to the coordination chemistry between AA and $HAuCl_4 \cdot 3H_2O$ solution (Murphy et al., 2011). Nevertheless, the bone-shaped Au NRs stand out for their significant shape and bigger size compared to all the previously described materials.

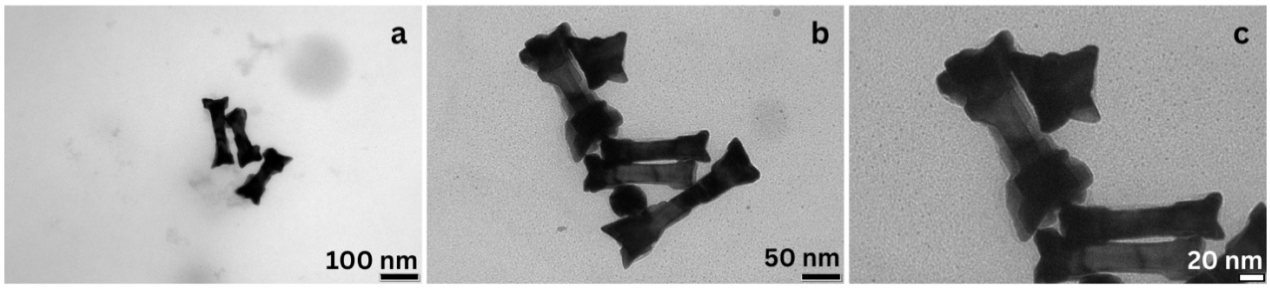

Figure 19. TEM Images of bone-shaped Au NRs.

Capsule-shaped gold core with platinum shell nanorods

Moving on to the first step of the capsule-shaped Au@Pt NRs, the capsule-shaped Au NRs shown in Figure 20. The name “capsule-shaped”, used for the rest of steps in this synthesis process, comes from their resemblance to a medicine capsule since it is an elongated rectangle with curved edges. The shape of the capsule-shaped Au NRs differs from their precursor Au Ps which consists mainly of spherical structures. On the other hand, the size of within the capsule-shaped Au NRs remains constant in their majority with slight exceptions.

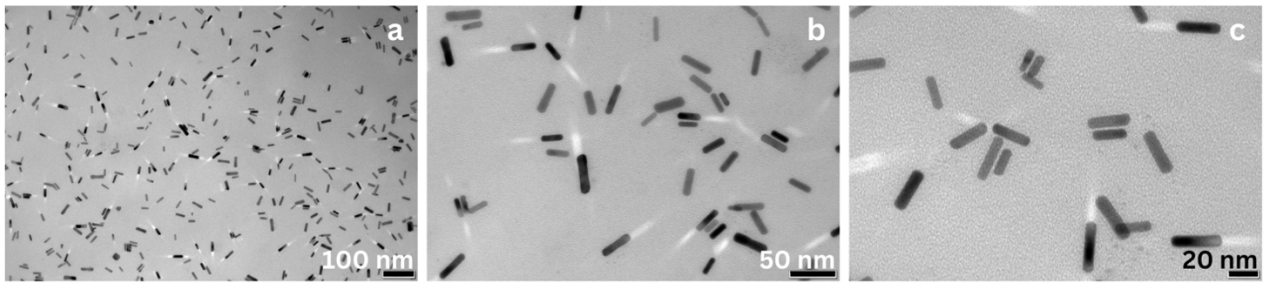

Figure 20. TEM Images of capsule-shaped Au NRs.

Moving on to the second step in the synthesis of capsule-shaped Au@Pt NRs, Au@Ag NRs is visualized in Figure 21. As it can be appreciated in the figure, the shape of the capsule-shaped Au@Ag NRs can still be considered as a capsule-like structure, but it changes slightly due to the silver (Ag) coating over the Au NRs that also causes a slight change in the size of the nanostructure. At the same time, the surface from the capsule-shaped Au@Ag NRs is not as smooth as the one seen in the capsule-shaped Au NRs in Figure 20 result of the silver coating.

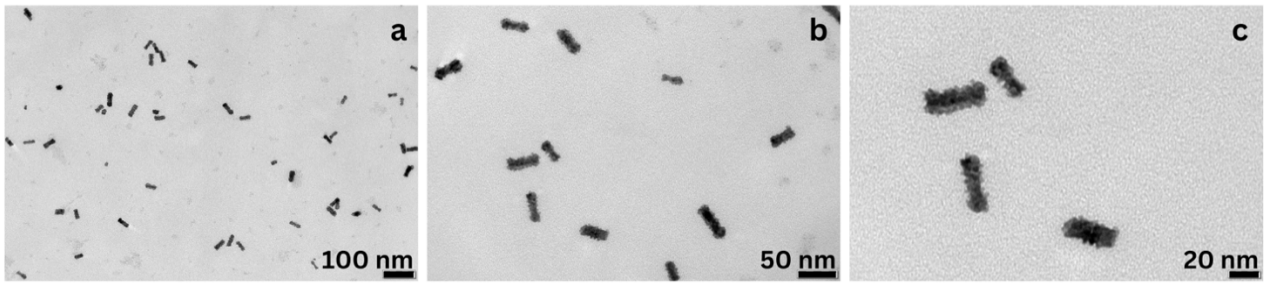

Figure 21. TEM Images of capsule-shaped Au@Ag NRs.

In Figure 22, the Au@Pt-DC NRs are shown, the first type of synthesized capsule-shaped Au@Pt NRs. The Au@Pt-DC NRs were named as “hairy” due to their fuzzy looking structure visible in the figure below. The surface looks like this due to their discontinuous platinum (Pt) shell over the gold (Au) core; the dot-like pattern takes place because of the galvanic replacement without sulfuric acid. Comparing the other synthesis steps, shown in Figures 20-22, it is noticeable that both shape and sizes vary slightly among them. The three NRs have a capsule-shape structure, but their coatings make them seem slightly thicker or slimmer than the others, affecting their size in the process. The surface on Au@Pt-DC NRs even though it is “hairy” has a much more defined surface than the one seen on Au@Ag NRs.

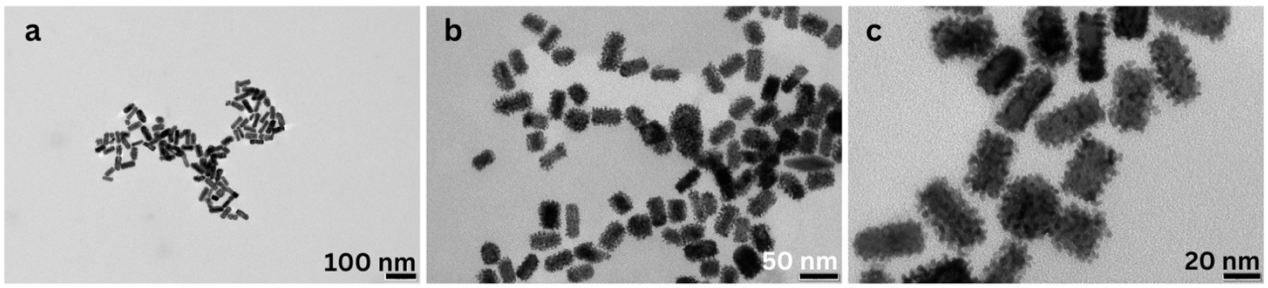

Figure 22. TEM Images of capsule-shaped Au@Pt-DC NRs.

The other type of capsule-shaped Au@Pt NRs, Au@Pt-C NRs, are seen on Figure 23. Their smooth surface gave them the name of “non hairy”, since it is compared to the surface seen on capsule-shaped “hairy” Au@Pt-DC NRs in Figure 22. Placing the “hairy” and “non hairy” side-to-side, it is noticeable that the continuous platinum (Pt) coating makes Au@Pt-C NRs show more defined edges and seem taller than the Au@Pt-DC NRs. On the other hand, when compared to the previous steps in the synthesis process, the capsule shape remains throughout all of them, but the edges and surfaces differ from each other. The smooth surface can be seen both in capsule-shaped Au NRs and Au@Pt-C NRs, yet the shape of the Au@Pt-C NRs is more rectangular than the ones of Au NRs. Darker contrast in the structures of capsule-shaped Au@Ag NRs and Au@Pt-C NRs can be seen, this is

related to the addition of a shell over the Au NRs. The surface of Au@Ag NRs seems fuzzier than the one in Au@Pt-C NRs, this is related to a thinner coating of metal over the core material.

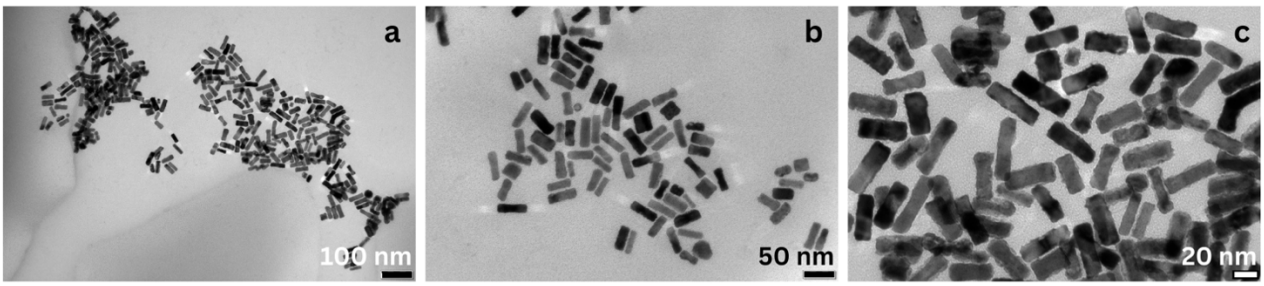

Figure 23. TEM Images of capsule-shaped Au@Pt-C NRs.

5.2 Electrochemical characterization

As it was mentioned before, CV is a powerful technique able to provide plenty of information regarding the ongoing redox reactions and other properties occurring between the components of an electrochemical cell and the analyte. For this study, CV was utilized to obtain information using a modified GCE behaviour in different analytes. The potential window under which the modified GCE remained stable will be studied first using PBS solution, moving on to the reversibility and redox reaction processes with $[Ru(NH_3)_6]Cl_3$ with KCl as buffer solution.

The following materials were used to modify the GCE and characterized with CV to address how their shapes affect the electrochemical behaviour: spherical Au NPs 3.3 AR, tooth-shaped Au NPs 2.1 AR, bone-shaped Au NRs, Au@Pt-DC NRs, Au@Pt-C NRs. The synthesized materials were separated into two categories, gold nanoparticles and core@shell nanorods. The first one composed by the nanostructures in which the main metallic component is gold (Au), such as spherical Au NPs 3.3 AR, tooth-shaped Au NPs 2.1 AR, and bone-shaped Au NRs. On the other hand, the core@shell nanorods were composed by capsule-shaped Au@Pt-DC and Au@Pt-C NRs. However, the same measurements were taken with an unmodified electrode on both categories to compare them with the ones of the other synthesized nanomaterials.

From all the CV measurements, the second curve was always chosen for analysis.

The five different types of synthesized NPs were characterized in more than one occasion, yielding comparable results and thereby confirming the reproducibility of the experiments.

5.2.1 Potential windows

As it can be appreciated in the Figures 24 and 25, the middle part of the set potential window remains constant with less than 1 μA current difference among the modified GCE, reason why the potential window was broadened until the current measurement values reached a value that reached or slightly surpassed the +/- 1 μA mark since a change of that magnitude was considered a much more significant change compared to the values seen in the middle part of the set potential window.

Gold nanoparticles

On Figure 24 shows the CV measurements comparing an unmodified GCE and of the Au NPs category to determine the potential windows under which the modified GCE was stable using all the synthesized nanomaterials in the category.

Starting with the unmodified GCE, it is noticeable that the middle part of the potential window has a higher capacitive current compared to the other NP samples. In this case, the potential window was broadened until a change in current of around +/- 1.5 μA was visualized. This change of values was seen when the potential ranged between 0 to 1 V.

Then, the GCE was modified with the spherical Au NPs 3.3 AR and a considerable change in the current values was seen with an estimated potential window between -0.3 – 1.1 V. Compared to the unmodified GCE, the spherical Au NPs 3.3 AR do not only exhibit a wider potential window but also seem to have lower background current values throughout the voltage path.

The GCE modified with tooth-shaped Au NPs 2.1 AR, showed a similar behaviour to the one exhibited by the spherical Au NPs 3.3 AR regarding the potential window range and low background current.

The final nanostructures in this category are the bone-shaped Au NRs. By modifying the GCE with bone-shaped Au NRs the potential window had significant changes in their current values in the potential window going from -0.2 V to 1.1 V. The path followed by this type of nanostructure follows the one seen by the spherical Au NPs 3.3 AR and tooth-shaped Au NPs 2.1 AR, even when the potential window is slightly smaller than the ones seen on the previous NPs. However, bone-shaped Au NRs had the lowest background current compared to the other NPs samples. The potential window variability can be related to the size of the NPs considering the size difference with the other Au NPs in this category seen in their previous characterization with TEM and UV-Vis.

Considering all the measurements seen in Figure 24, it is clear the Au NPs category offers more stability and wider potential window than the unmodified GCE. However, it would be necessary to repeat the measurement conducted with the GCE modified with bone-shaped Au NRs since the negative potential is not as marked as the one seen with the other Au NPs.

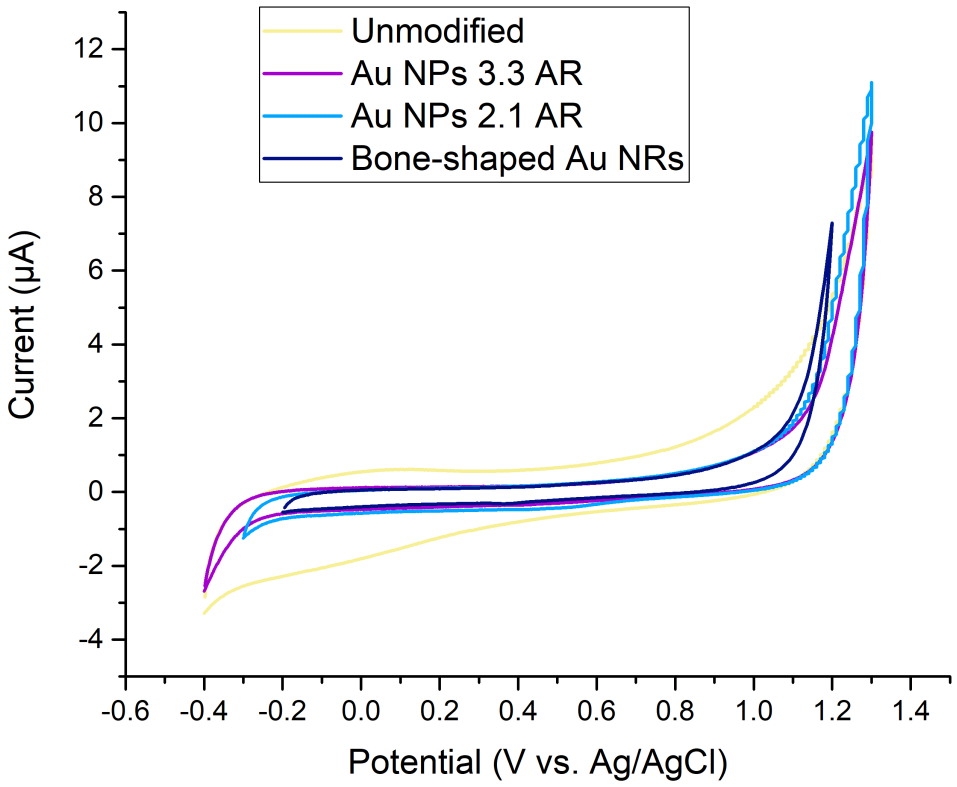

Figure 24. CV of GCE unmodified and modified with spherical Au NPs 3.3 AR, tooth-shaped Au NPs 2.1 AR, and bone-shaped Au NRs in PBS solution.

Capsule-shaped gold core with platinum shell nanorods

Figure 25 shows the CV measurements of the core@shell NRs category to determine the potential windows under which a modified GCE with these NRs remains stable and compares it to an unmodified GCE.

A higher capacitive current is seen with the unmodified GCE by looking at the middle part of the potential window when compared to the other NPs samples. This potential window was broadened until the current measurement changed around +/- 1.5 µA, which were seen between the potential values of 0 V and 1 V.

The first modification took place with capsule-shaped Au@Pt-DC NRs, which exhibited a very stable current measurements as the potential window was ran in the experiment, until significant changes were seen on the potential window set in between the values of -0.3 V and 1.2 V. The stability stands out when compared to the measured values of the unmodified GCE, yet the potential window is also wider for the “hairy” NRs.

Moving on to the GCE modification done with capsule-shaped Au@Pt-C NRs, this type of NRs exhibit a thicker measurement in their middle potential values. Yet, a considerable change in the measured current values was seen with the potential window set in between 0 – 0.9 V. These values are slightly smaller than the ones exhibited by the capsule-shaped Au@Pt-DC NRs, but this could have occurred due to the shell composition since gold (Au) is known to be a more conductive material compared to platinum (Pt).

Figure 25 shows that using core@shell NRs for electrode modification has an impact on the potential window, since by looking at the figure different windows can be spotted. When compared to an unmodified GCE, both core@shell NRs showed lower capacitive currents, yet the modification done with Au@Pt-DC NRs had the lowest value in this category.

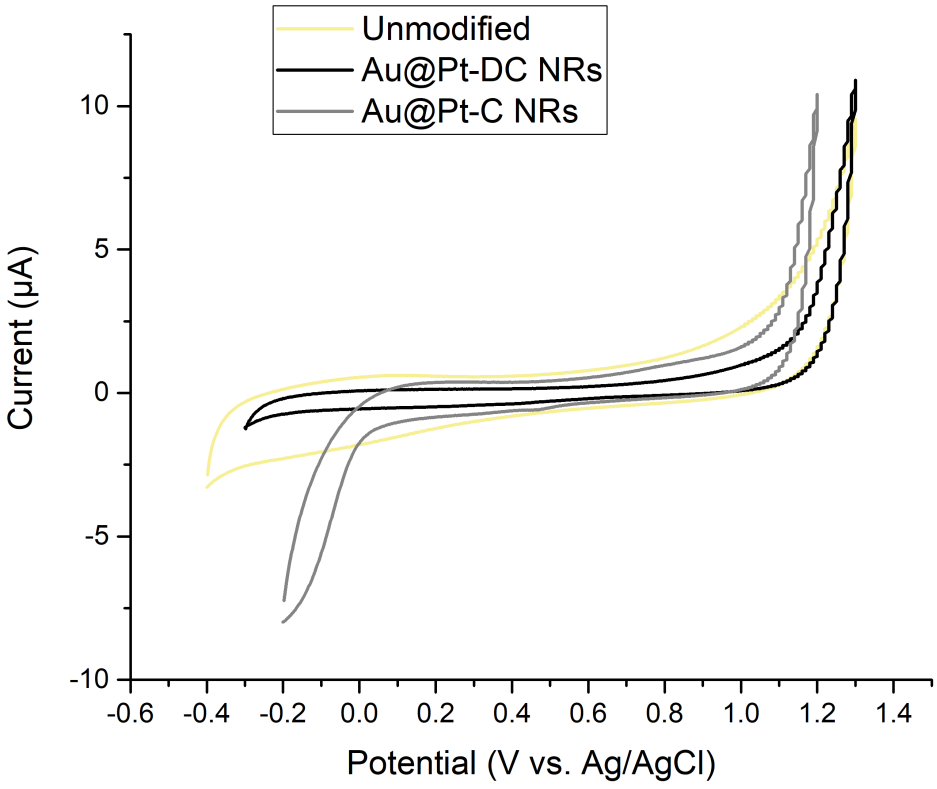

Figure 25. CV of GCE unmodified and modified with Au@Pt-DC NRs and Au@Pt-C NRs in PBS solution.

5.2.2 Outer sphere redox probe studies

In the experimental section it was mentioned that measurements were done with three different scan rates: 400 mV/s^{-1}, 200 mV/s^{-1}, and 50 mV/s^{-1}. The chosen scan rate for the Figures 26 and 27 was 400 mV/s^{-1}. These CV measurements seen below aim to obtain information about the reversibility and redox reaction processes.

Gold nanoparticles

The CV measurements comparing an unmodified GCE and modified GCE with the NPs in the Au NPs category are shown in Figure 26.

An oxidation and reduction peak were clearly visible with the unmodified GCE, and measurements made with the other 3 types of synthesized NPs. The spherical and tooth-shaped Au NPs had their peaks at the same potential value as the unmodified GCE but showed lower current values as well. This could have been caused due to the different shape and size from the NPs, as well as to the measured signal being affected by the concentration of nanomaterials found on the surface. Considering that the size difference is not as abrupt between the spherical and tooth-shaped Au NPs, the proximity on the measured current values can be explained.

On the other hand, the bone-shaped Au NRs modified measurements did not only seem to have a different oxidation and reduction peak potential position, but their peak current values are significantly lower to the ones seen in an unmodified GCE. These difference in potential peaks and current values is also seen with the other types of NPs, but the bigger difference is appreciated with the unmodified GCE. This could also be a result of the much bigger size of the bone-shaped Au NRs and concentration difference of the nanostructure in the surface of the electrode. The TEM characterization can confirm that the size difference between the bone-shaped Au NRs and the different aspect ratio NPs is significant and could be a potential reason why the measurements differ among the characterized types of NPs in this category.

Nevertheless, after looking at the measurements made in the Au NPs category, it is noticeable that modifying a GCE with Au NPs alters the electrochemical behaviour. The response varies depending on the shape and size of the nanomaterial, yet it can be considered that the background noise also gets reduced by modifying the surface of the GCE.

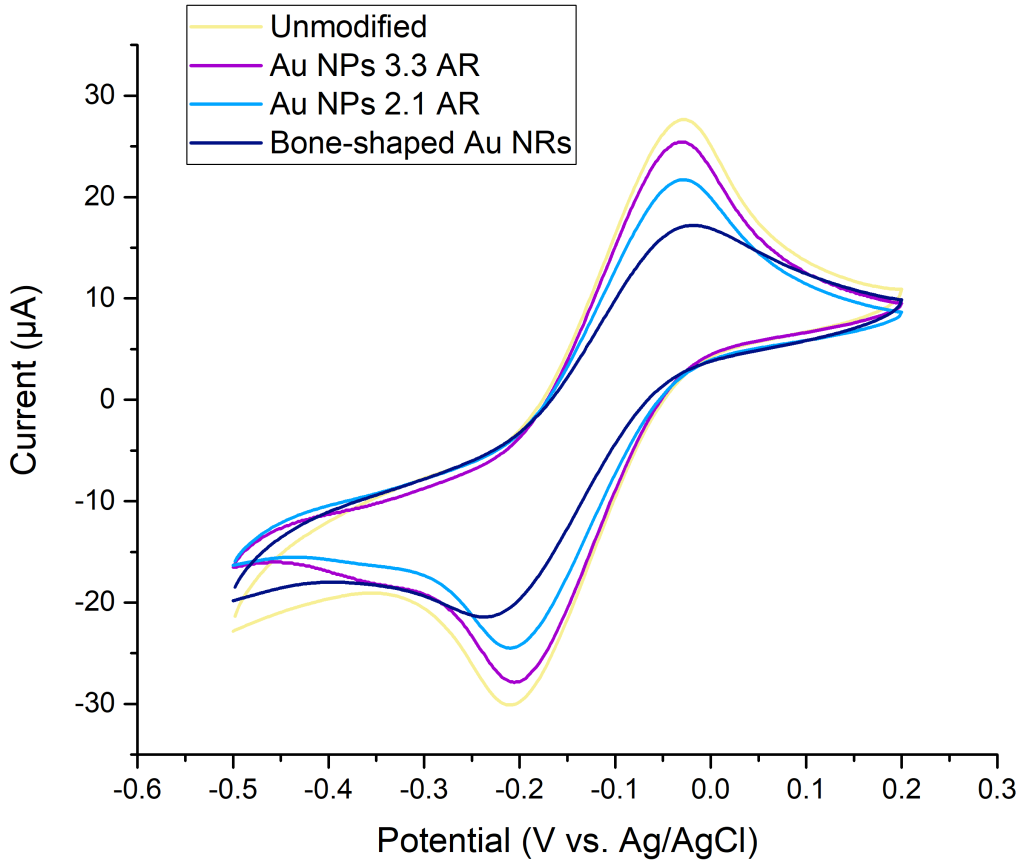

Figure 26. CV measurements of GCE unmodified and modified with spherical Au NPs 3.3 AR, tooth-shaped Au NPs 2.1 AR, and bone-shaped Au NRs in $[Ru(NH_3)]_6Cl_3$ with KCl as buffer solution.

Capsule-shell gold core with platinum shell nanorods

Figure 27 visualizes the CV measurements of an unmodified and modified GCE with the NRs in the core@shell NRs category.

An oxidation and reduction peak were clearly visible with the measurements made with the unmodified GCE, and the ones done with both types of Au@Pt NRs. The peaks were found at the same potential value, but they differed slightly on the current values.

Unlike the measurements observed in Figure 26 of the Au NPs category, the current peak values for the two types of Au@Pt NRs were identical. Indicating that the difference becomes apparent only when compared to the peak current value seen on the unmodified GCE.

The measurements made with the NPs in the core@shell category showed excellent outer sphere redox probe behaviour regardless of the NRs used, with minimal change in the electrochemical behaviour showing that Au@Pt NRs have a similar response to the one seen in an unmodified GCE.

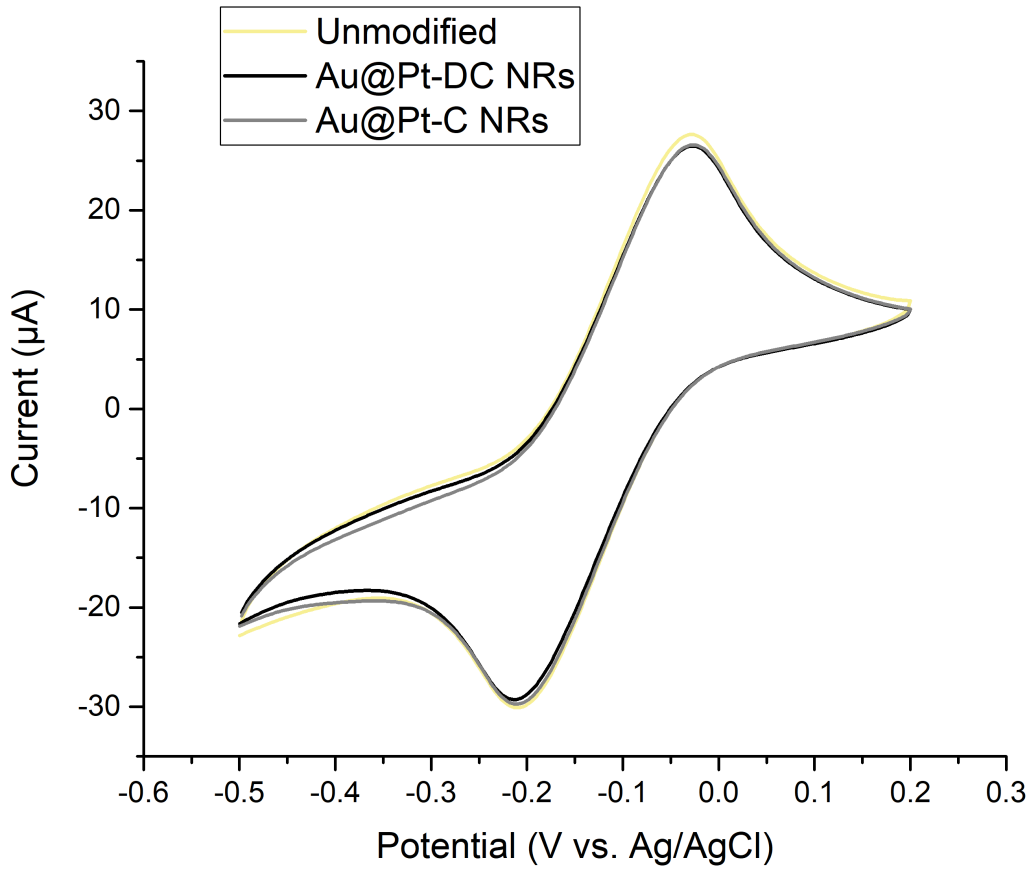

Figure 27. CV measurements of GCE unmodified and modified with capsule-shaped Au@Pt-DC NRs and Au@Pt-C NRs in $[Ru(NH_3)]_6Cl_3$ with KCl as buffer solution.

6 Conclusion

This thesis aimed to synthesize various types of metallic NPs by controlling their size, shape, and composition to study their electrochemical behaviour when used to modify a GCE.

The synthesis process was successful for all desired types of NPs, as different shapes, sizes, and compositions were achieved. This was confirmed by characterizing the synthesized NPs using UV-Vis, and TEM.

All synthesized NPs were used to modify a GCE, which was then characterized electrochemically using CV. The electrochemical characterization helped defining the potential window and the behaviour of the outer sphere redox probe. The results showed that modifying the GCE with the different synthesized metallic NPs changes the electrode's behaviour compared to an unmodified GCE. Comparing the 5 characterized NPs, it was noticeable that bigger sized NPs tended to result in lower peak currents and that using Au NPs with platinum (Pt) shells did not change the behaviour of the GCE significantly.

The synthesis processes and electrochemical studies are reproducible, since they were repeated multiple times with consistent results.

However, the synthesis and characterization of the various types of synthesized Au NPs can be enhanced by controlling better the conditions under which the NPs are fabricated. Since the process and end results are highly sensitive to the quality of the used chemicals and the amount of compound added to the solutions.

The experiments and research conducted in this thesis have potential for further studies of the electrochemical behaviour caused by the synthesized metallic NPs used to modify a GCE. The interaction of the electrode with different analytes including biomolecules, modifying further the surface of the electrode or by placing the NPs in specific positions could be of interest for biosensing applications.

References

Alexis, F., Pridgen, E., Molnar, L.K., Farokhzad, O.C., 2008. Factors Affecting the Clearance and Biodistribution of Polymeric Nanoparticles. Mol. Pharm. 5, 505–515. https://doi.org/10.1021/mp800051m

Ali, M.R.K., Snyder, B., El-Sayed, M.A., 2012. Synthesis and Optical Properties of Small Au Nanorods Using a Seedless Growth Technique. Langmuir 28, 9807–9815. https://doi.org/10.1021/la301387p

Alim, S., Vejayan, J., Yusoff, M.M., Kafi, A.K.M., 2018. Recent uses of carbon nanotubes & gold nanoparticles in electrochemistry with application in biosensing: A review. Biosens. Bioelectron. 121, 125–136. https://doi.org/10.1016/j.bios.2018.08.051

Burda, C., Chen, X., Narayanan, R., El-Sayed, M.A., 2005. Chemistry and Properties of Nanocrystals of Different Shapes. Chem. Rev. 105, 1025–1102. https://doi.org/10.1021/cr030063a

Chan, W.C.W. (Ed.), 2007. Bio-applications of nanoparticles, Advances in experimental medicine and biology. Springer Science + Business Media ; Landes Bioscience, [New York] : Austin, Tex.

Chen, G., Qiu, H., Prasad, P.N., Chen, X., 2014. Upconversion Nanoparticles: Design, Nanochemistry, and Applications in Theranostics. Chem. Rev. 114, 5161–5214. https://doi.org/10.1021/cr400425h

Cheong, S., Ferguson, P., Feindel, K.W., Hermans, I.F., Callaghan, P.T., Meyer, C., Slocombe, A., Su, C., Cheng, F., Yeh, C., Ingham, B., Toney, M.F., Tilley, R.D., 2011. Simple Synthesis and Functionalization of Iron Nanoparticles for Magnetic Resonance Imaging. Angew. Chem. Int. Ed. 50, 4206–4209. https://doi.org/10.1002/anie.201100562

Cobley, C.M., Xia, Y., 2010. Engineering the properties of metal nanostructures via galvanic replacement reactions. Mater. Sci. Eng. R Rep. 70, 44–62. https://doi.org/10.1016/j.mser.2010.06.002

Dreaden, E.C., Alkilany, A.M., Huang, X., Murphy, C.J., El-Sayed, M.A., 2012. The golden age: gold nanoparticles for biomedicine. Chem Soc Rev 41, 2740–2779. https://doi.org/10.1039/C1CS15237H

Elgrishi, N., Rountree, K.J., McCarthy, B.D., Rountree, E.S., Eisenhart, T.T., Dempsey, J.L., 2018. A Practical Beginner's Guide to Cyclic Voltammetry. J. Chem. Educ. 95, 197–206. https://doi.org/10.1021/acs.jchemed.7b00361

Espinoza, E.M., Clark, J.A., Soliman, J., Derr, J.B., Morales, M., Vullev, V.I., 2019. Practical Aspects of Cyclic Voltammetry: How to Estimate Reduction Potentials When Irreversibility Prevails. J. Electrochem. Soc. 166, H3175–H3187. https://doi.org/10.1149/2.0241905jes

Fennell, J., He, D., Tanyi, A.M., Logsdail, A.J., Johnston, R.L., Li, Z.Y., Horswell, S.L., 2013. A Selective Blocking Method To Control the Overgrowth of Pt on Au Nanorods. J. Am. Chem. Soc. 135, 6554–6561. https://doi.org/10.1021/ja4003475

Gou, L., Murphy, C.J., 2005. Fine-Tuning the Shape of Gold Nanorods. Chem. Mater. 17, 3668–3672. https://doi.org/10.1021/cm050525w

Grieshaber, D., MacKenzie, R., Vörös, J., Reimhult, E., 2008. Electrochemical Biosensors - Sensor Principles and Architectures. Sensors 8, 1400–1458. https://doi.org/10.3390/s80314000

Guo, S., Wang, L., Wang, Y., Fang, Y., Wang, E., 2007. Bifunctional Au@Pt hybrid nanorods. J. Colloid Interface Sci. 315, 363–368. https://doi.org/10.1016/j.jcis.2007.06.022

Hajihosseini, S., Nasirizadeh, N., Hejazi, M.S., Yaghmaei, P., 2016. A sensitive DNA biosensor fabricated from gold nanoparticles and graphene oxide on a glassy carbon electrode. Mater. Sci. Eng. C 61, 506–515. https://doi.org/10.1016/j.msec.2015.12.091

Huang, X., El-Sayed, I.H., Qian, W., El-Sayed, M.A., 2006. Cancer Cell Imaging and Photothermal Therapy in the Near-Infrared Region by Using Gold Nanorods. J. Am. Chem. Soc. 128, 2115–2120. https://doi.org/10.1021/ja057254a

Huang, X., Neretina, S., El-Sayed, M.A., 2009. Gold Nanorods: From Synthesis and Properties to Biological and Biomedical Applications. Adv. Mater. 21, 4880–4910. https://doi.org/10.1002/adma.200802789

Jelinek, R., 2015. Nanoparticles. Walter de Gruyter, Berlin.

Jing, H., Zhang, Q., Large, N., Yu, C., Blom, D.A., Nordlander, P., Wang, H., 2014. Tunable Plasmonic Nanoparticles with Catalytically Active High-Index Facets. Nano Lett. 14, 3674–3682. https://doi.org/10.1021/nl5015734

Joudeh, N., Linke, D., 2022. Nanoparticle classification, physicochemical properties, characterization, and applications: a comprehensive review for biologists. J. Nanobiotechnology 20, 262. https://doi.org/10.1186/s12951-022-01477-8

Khan, Ibrahim, Saeed, K., Khan, Idrees, 2019. Nanoparticles: Properties, applications and toxicities. Arab. J. Chem. 12, 908–931. https://doi.org/10.1016/j.arabjc.2017.05.011

Khoshroo, A., Hosseinzadeh, L., Sobhani-Nasab, A., Rahimi-Nasrabadi, M., Ehrlich, H., 2018. Development of electrochemical sensor for sensitive determination of oxazepam based on silver-platinum core–shell nanoparticles supported on graphene. J. Electroanal. Chem. 823, 61–66. https://doi.org/10.1016/j.jelechem.2018.05.030

Kim, D., Kim, J., Park, Y.I., Lee, N., Hyeon, T., 2018. Recent Development of Inorganic Nanoparticles for Biomedical Imaging. ACS Cent. Sci. 4, 324–336. https://doi.org/10.1021/acscentsci.7b00574

Kim, F., Song, J.H., Yang, P., 2002. Photochemical Synthesis of Gold Nanorods. J. Am. Chem. Soc. 124, 14316–14317. https://doi.org/10.1021/ja028110o

Kong, F.-Y., Gu, S.-X., Li, W.-W., Chen, T.-T., Xu, Q., Wang, W., 2014. A paper disk equipped with graphene/polyaniline/Au nanoparticles/glucose oxidase biocomposite modified screen-printed electrode: Toward whole blood glucose determination. Biosens. Bioelectron. 56, 77–82. https://doi.org/10.1016/j.bios.2013.12.067

Liu, Guyot-Sionnest, P., 2004. Synthesis and Optical Characterization of Au/Ag Core/Shell Nanorods. J. Phys. Chem. B 108, 5882–5888. https://doi.org/10.1021/jp037644o

Lohse, S.E., Murphy, C.J., 2013. The Quest for Shape Control: A History of Gold Nanorod Synthesis. Chem. Mater. 25, 1250–1261. https://doi.org/10.1021/cm303708p

Ma, H., Yin, B., Wang, S., Jiao, Y., Pan, W., Huang, S., Chen, S., Meng, F., 2004. Synthesis of Silver and Gold Nanoparticles by a Novel Electrochemical Method. ChemPhysChem 5, 68–75. https://doi.org/10.1002/cphc.200300900

Malekzad, H., Sahandi Zangabad, P., Mirshekari, H., Karimi, M., Hamblin, M.R., 2017. Noble metal nanoparticles in biosensors: recent studies and applications. Nanotechnol. Rev. 6, 301–329. https://doi.org/10.1515/ntrev-2016-0014

Malhotra, B.D., Ali, Md.A., 2018. Nanomaterials in Biosensors, in: Nanomaterials for Biosensors. Elsevier, pp. 1–74. https://doi.org/10.1016/B978-0-323-44923-6.00001-7

Miao, Z., Wang, P., Zhong, A., Yang, M., Xu, Q., Hao, S., Hu, X., 2015. Development of a glucose biosensor based on electrodeposited gold nanoparticles–polyvinylpyrrolidone–polyaniline nanocomposites. J. Electroanal. Chem. 756, 153–160. https://doi.org/10.1016/j.jelechem.2015.08.025

Murphy, C.J., Thompson, L.B., Chernak, D.J., Yang, J.A., Sivapalan, S.T., Boulos, S.P., Huang, J., Alkilany, A.M., Sisco, P.N., 2011. Gold nanorod crystal growth: From seed-mediated synthesis to nanoscale sculpting. Curr. Opin. Colloid Interface Sci. 16, 128–134. https://doi.org/10.1016/j.cocis.2011.01.001

Najahi-Missaoui, W., Arnold, R.D., Cummings, B.S., 2020. Safe Nanoparticles: Are We There Yet? Int. J. Mol. Sci. 22, 385. https://doi.org/10.3390/ijms22010385

Njoki, P.N., Lim, I.-I.S., Mott, D., Park, H.-Y., Khan, B., Mishra, S., Sujakumar, R., Luo, J., Zhong, C.-J., 2007. Size Correlation of Optical and Spectroscopic Properties for Gold Nanoparticles. J. Phys. Chem. C 111, 14664–14669. https://doi.org/10.1021/jp074902z

Pérez-Juste, J., Pastoriza-Santos, I., Liz-Marzán, L.M., Mulvaney, P., 2005. Gold nanorods: Synthesis, characterization and applications. Coord. Chem. Rev. 249, 1870–1901. https://doi.org/10.1016/j.ccr.2005.01.030

Rabbani, G., Khan, M.E., Khan, A.U., Ali, S.K., Zamzami, M.A., Ahmad, A., Bashiri, A.H., Zakri, W., 2024. Label-free and ultrasensitive electrochemical transferrin detection biosensor based on a glassy carbon electrode and gold nanoparticles. Int. J. Biol. Macromol. 256, 128312. https://doi.org/10.1016/j.ijbiomac.2023.128312

Saha, K., Agasti, S.S., Kim, C., Li, X., Rotello, V.M., 2012. Gold Nanoparticles in Chemical and Biological Sensing. Chem. Rev. 112, 2739–2779. https://doi.org/10.1021/cr2001178

Scarabelli, L., Sánchez-Iglesias, A., Pérez-Juste, J., Liz-Marzán, L.M., 2015. A "Tips and Tricks" Practical Guide to the Synthesis of Gold Nanorods. J. Phys. Chem. Lett. 6, 4270–4279. https://doi.org/10.1021/acs.jpclett.5b02123

Sekretaryova, A.N., Eriksson, M., Turner, A.P.F., 2016. Bioelectrocatalytic systems for health applications. Biotechnol. Adv. 34, 177–197. https://doi.org/10.1016/j.biotechadv.2015.12.005

Shanbhag, M.M., Manasa, G., Mascarenhas, R.J., Mondal, K., Shetti, N.P., 2023. Fundamentals of bio-electrochemical sensing. Chem. Eng. J. Adv. 16, 100516. https://doi.org/10.1016/j.ceja.2023.100516

Sharma, V., Sinha, N., Dutt, S., Chawla, M., Siril, P.F., 2016. Tuning the surface enhanced Raman scattering and catalytic activities of gold nanorods by controlled coating of platinum. J. Colloid Interface Sci. 463, 180–187. https://doi.org/10.1016/j.jcis.2015.10.036

Srnová-Šloufová, I., Vlčková, B., Bastl, Z., Hasslett, T.L., 2004. Bimetallic (Ag)Au Nanoparticles Prepared by the Seed Growth Method: Two-Dimensional Assembling, Characterization by Energy Dispersive X-ray Analysis, X-ray Photoelectron Spectroscopy, and Surface Enhanced Raman Spectroscopy, and Proposed Mechanism of Growth. Langmuir 20, 3407–3415. https://doi.org/10.1021/la0302605

St. Angelo, S.K., 2014. TEM for Characterization of Nanowires and Nanorods, in: Kumar, C.S.S.R. (Ed.), Transmission Electron Microscopy Characterization of Nanomaterials. Springer Berlin Heidelberg, Berlin, Heidelberg, pp. 195–241. https://doi.org/10.1007/978-3-642-38934-4_5

Sztandera, K., Gorzkiewicz, M., Klajnert-Maculewicz, B., 2019. Gold Nanoparticles in Cancer Treatment. Mol. Pharm. 16, 1–23. https://doi.org/10.1021/acs.molpharmaceut.8b00810

Tan, K.X., Barhoum, A., Pan, S., Danquah, M.K., 2018. Risks and toxicity of nanoparticles and nanostructured materials, in: Emerging Applications of Nanoparticles and Architecture

Nanostructures. Elsevier, pp. 121–139. https://doi.org/10.1016/B978-0-323-51254-1.00005-1

Teymourian, H., Barfidokht, A., Wang, J., 2020. Electrochemical glucose sensors in diabetes management: an updated review (2010–2020). Chem. Soc. Rev. 49, 7671–7709. https://doi.org/10.1039/D0CS00304B

Toshima, N., Yonezawa, T., 1998. Bimetallic nanoparticles—novel materials for chemical and physical applications. New J. Chem. 22, 1179–1201. https://doi.org/10.1039/a805753b

Vigderman, L., Khanal, B.P., Zubarev, E.R., 2012. Functional Gold Nanorods: Synthesis, Self-Assembly, and Sensing Applications. Adv. Mater. 24, 4811–4841. https://doi.org/10.1002/adma.201201690

Wang, Y., Wang, C., 2014. TEM for Characterization of Core-Shell Nanomaterials, in: Kumar, C.S.S.R. (Ed.), Transmission Electron Microscopy Characterization of Nanomaterials. Springer Berlin Heidelberg, Berlin, Heidelberg, pp. 243–285. https://doi.org/10.1007/978-3-642-38934-4_6

Yih, T.C., Talpasanu, I. (Eds.), 2008. Micro and nano manipulations for biomedical applications. Artech House, Boston, MA.

Zhou, Z., Sun, Y., Shen, J., Wei, J., Yu, C., Kong, B., Liu, W., Yang, H., Yang, S., Wang, W., 2014. Iron/iron oxide core/shell nanoparticles for magnetic targeting MRI and near-infrared photothermal therapy. Biomaterials 35, 7470–7478. https://doi.org/10.1016/j.biomaterials.2014.04.063